International Journal of Science and Research (IJSR)
ISSN (Online): 2319-7064
Index Copernicus Value (2013): 6.14 | Impact Factor (2015): 6.391

Determination of Structural and Vibrational Spectroscopic Properties of 4-Amino-2, 2, 6, 6-tetramethylpiperidine using FT-IR and FT-Raman Experimental Techniques and Quantum Chemical Calculations

G. Mahalakshmi[1], R. Suganya[2], V. Balachandran[3]

[1, 2]Research Department of Physics, Government Arts College (Autonomou), Karur-639 001, India

[3]Research Department of Physics, A A Government Arts College, Musiri 621 211, India

Abstract: ***In this work, the molecular conformation and vibrational analysis of 4-Amino-2, 2, 6, 6-tetramethylpiperidine (abbreviated as ATMP) were presented for the ground state using experimental techniques (FT-IR and FT-Raman) and the spectra were interpreted with the aid of normal coordinate analysis based on ab initio Hartree−Fock (HF) and density functional theory (DFT/B3LYP) methods with 6-311+G (d, p) basis set level. The statistical thermodynamic functions (heat capacity, entropy change, enthalpy change and free energy change) were obtained. The polarizability, first hyperpolarizability, anisotropy polarizability invariant has been computed using quantum chemical calculations. The infrared and Raman spectra were also predicted from the calculated intensities. Comparison of the experimental and theoretical spectra values provides important information about the ability of the computational method to describe the vibrational modes. UV-VIS spectral analyses of ATMP have been researched by theoretical calculations. In order to understand electronic transitions of the compound, TD-DFT calculations on electronic absorption spectra in gas phase and solvent (DMSO and Chloroform) were performed. The calculated frontier orbital energies, excitation energies (E), absorption wavelengths (λ), os cillator strengths (f) and life span(τ) for gas phase and solvent (DMSO and Chloroform) are also illustrated.***

Keywords: Vibrational spectra, TD-DFT, Fukui function, NBO analysis, Thermodynamic functions

1. Introduction

Piperidine is widely used as a building block and chemical reagent in the synthesis of organic compounds including pharmaceuticals. It is used as a secondary amine and to convert ketone to enamines [1]. Enamines are derived from piperidine which are used in the stork enamines alkylatinereactions [2]. Piperidine can be converted to the chloroamines $C_5H_{10}NCl$ with calcium hypochlorite [3]. It is also commonly used in chemical degradation reactions. Pyridine can also be reduced to piperidine by sodium in ethanol [4]. Piperidine and its derivatives are very important in industrial field as well as in biochemistry. The piperidine structural motives are present in numerous natural alkaloids. Piperidine itself has been obtained from black pepper, psilocaulonabsimile and N.E.Br (Aizoaceae) and in petrosimoniamonandra [5, 6, 7]. Other examples are the fire ant toxin solenopsin [8], the nicotin, analog anabasine of the tree tobacco (nicotianaglauca), lobeline of the Indian tobacco and the toxic alkaloid coniine from poison hemlock which was used to put Socrates to death [9].

Piperidine is used as solvent and as a base. The same is true for certain derivatives of N-formylpiperidine which is a polar aprotic solvent with better hydrocarbon solubility than other amide solvents and 2,2,6,6-tetramethyl piperidine is a highly sterically hindered base, useful because of its low nucleophilicity and high solubility in organic solvents. Piperidine, hexahydropyridine is a family of heterocyclic organic compounds derived from pyridine through hydrogenation. It has one nitrogen atom in the cycle. It has clear liquid with pepper like aroma. The major application of piperidine is the production of dipiperidinyldithiuramtetrasulphide used as a rubber vulcanization accelerator [10].

In pharmaceutical synthesis industries, it is a skeleton in some drugs such as methyl phenidate [central nervous system stimulant], budipine [antiparkinsonian drug], raloxifene, minoxidil [an oral drug to treat high blood pressure]. It is used as special solvent in solid base synthesis and protections to make crystal derivatives of aromatic nitrogen compounds containing nuclear halogen atoms. Ring system compounds with nitrogen which have basics property playing important roles of cyclic components in industrial field such as raw materials for hardness of epoxy resins. Corrosion inhibitor, insecticides, accelerators are used as rubber urethane catalysts antioxidants and as a catalyst for silicone esters. They are used in manufacturing pharmaceuticals.

The main objective of the present study is to investigate in detail about the conformational stability and vibrational spectra of 4-Amino-2, 2, 6, 6-tetramethylpiperidine (ATMP) using DFT methods which can presumably helps in understanding its dynamical behavior. The characterization of the normal modes using potential energy distribution is done with the MOLVIB-7.0 program. In the present work we have attempted to study the bonding nature of ATMP using B3LYP level of theory throughout with the 6-311+G(d,p) basis set implemented in the Gaussian 09

program [11] from the DFT calculation were then used to perform natural bond orbital (NBO) analysis.

Literature survey reveals that to the best of our knowledge, the spectroscopic characterization and quantum chemical calculations of charge transfer, MEP, thermo-chemical analysis and solvent effects on the title molecule have no reports. Therefore, the present investigation was undertaken to study the geometric structure and vibrational spectra of ATMP. The FT-IR and FT-Raman experimental techniques were recorded and interpreted in terms of calculated ones at DFT with B3LYP/6-311+G (d, p) level. A detailed interpretation of the vibrational spectra of title molecules was made on the basis of the calculated total energy distribution (TED) results.

2. Methodology

Experimental details

Samples in liquid form were purchased from the Lancaster Chemical Company (UK) with a purity of greater than 98%, and they were used as such without purification. FT-IR spectra of the compound was recorded in the region 400–4000 cm^{-1} on a BRUKER spectrophotometer equipped with an MCT detector, in KBr pellet. FT-Raman spectra of ATMP have been recorded in the region 100–3500 cm^{-1}on a BRUKER spectrophotometer equipped with Raman module accessory with Nd:YAG laser operating at 1.5 W powers continuously with 1064 nm excitation.

Quantum chemical calculation (computational)

The first task for the computational work was to determine the optimized geometry, energy and vibrational frequencies of the compound have been calculated by using B3 [12] exchange functional combined with the LYP [13] correlation functional resulting in the B3LYP density functional method at 6-311+G (d, p) basis set. All the computations were performed using Gaussian 09W program [11] and Gauss-View molecular visualization program package on the personal computer [14]. Second, a comparison is made between the theoretically calculated wavenumbers and the experimentally measured wavenumbers. In this investigation we observed that the calculated wavenumbers were slightly greater than the fundamental wavenumbers. To improve the agreement between the predicted and observed wavenumbers, the computed harmonic wavenumbers are usually scaled for comparison. For this purpose the scaling of the force field was performed according to the SQMFF procedure [15]. The Cartesian representation of the force constants were transferred to a non-redundant set of local symmetry coordinates, chosen in accordance to recommendations of Pulay *et al* [16]. The descriptions of the predicted frequencies during the scaling process were followed by the total energy distribution (TED) matrix. The characterization of the normal modes using total energy distribution (TED) was done with the MOLVIB – 7.0 programs written by Sundius [17, 18]. The NBO calculations [19] were performed using NBO program as carried out in the Gaussian 09W [11] package at the DFT/B3LYP level to understand the intra-molecular delocalization or hyper-conjugation.

The frontier molecular orbital energies, energy gap between various occupied and unoccupied molecular orbital's of ATMP are also calculated in the same method with different basis sets. NBO calculation is also performed on the ATMP with the same level of DFT theory with 6-311+G (d, p) basis set. For obtaining chemical reactivity of the molecule, the molecular electrostatic potential (MEP) surface is plotted over the optimized geometry of ATMP using Gaussian 09W software package [11]. The fitting point charges to electrostatic potential on each atom of the optimized geometry are compared with MEP surface. Moreover, Mulliken atomic charges of atoms and certain thermodynamic properties such as entropy, enthalpy, rotational constants, vibrational constants, and zero point vibrational energy of the title compound are also calculated at the same level of DFT calculation. Thermo chemical calculation was done by employing vibrational frequencies at B3LYP/6-311+G (d, p) level of theory.

Net atomic charges have been obtained using the natural population analysis scheme of Reed *et al*. [20]. The electronic structure and bonding features of the compounds studied were analyzed using natural bond orbital analysis [20, 21]. The natural bond orbital analysis allowed us to describe the bonding in terms of the natural hybrids centered on each atom. For estimation of the probable reactive sites in the systems studied, two molecular descriptors were used viz; MEP and Fukui functions. MEP is related to electronic density and is considered as a fundamental determinant of atomic and molecular properties. Therefore, MEP has largely been used as a molecular descriptor of the chemical reactivity of number of biological systems, which take part in both electrophilic and nucleophilic reactions as well as hydrogen bonding interactions [22, 23]. The molecular electrostatic potential *V(r)*, at a given point *r(x, y, z)* in the vicinity of a molecule, is defined in terms of the interaction energy between the electrical charge generated from the molecule electrons and nuclei and a positive test charge (a proton) located at *r* . For the systems studied the MEP values were calculated using the equation [24].

$$V(r) = \sum \frac{Z_A}{|R_A - r|} - \int \frac{\rho(r')}{|r' - r|} dr$$

where the summation runs over all the nuclei *A* in the compound and polarization and reorganization effects is neglected. Z_A is the charge of the nucleus *A*, located at R_A and $\rho(r')$ is the electron density function of the molecule.

The electronic properties, such as HOMO-LUMO energies, absorption wavelengths and oscillator strengths were calculated using B3LYP method of the time dependent TD-DFT, basing on the optimized structure in solvent (DMSO and Chloroform) and gas phase. The changes in the thermodynamic functions such as the heat capacity, entropy, and enthalpy were investigated for the different temperatures from the vibrational frequency calculations of the title molecule.

The prediction of Raman intensities and hyper-polarizability

The Raman activity (S_i) calculated by Gaussian 09 and adjusted during scaling procedure with MOLVIB were

converted to relative Raman intensity (I_i) using the following relation from the basic theory of Raman scattering [25, 26].

$$I_i = \frac{f(\nu_0 - \nu_i)^4 s_i}{\nu_i\left[1 - \exp\left(\frac{-hc\nu_i}{k_b T}\right)\right]}$$

Here ν_0 is the laser exciting frequency in cm^{-1} units (in this work, we have used the excitation wavenumber ν_0 = 9398 cm^{-1}, which corresponds to the wavelength of 1064nm of a Nd: YAG laser), ν_i is the vibrational wavenumbers of the i^{th} normal mode (cm^{-1}): h, k_b, c are Planck, Boltzmann constants, speed of light , T is the temperature in Kelvin, and f (is a constant equal to 10^{-12}) is the suitably chosen common normalization factor for all the peak intensities.

Analysis of organic compounds having conjugated π - electron systems and large hyper-polarizability using IR and Raman spectroscopy has evolved as a subject of research. The potential application of the title compound in the field of non-linear optics demands the investigation of its structural and bonding features contributing to the hyper-polarizability enhancement by analyzing the vibrational modes using IR and Raman spectroscopy. The B3LYP/6-311+G (d, p) method has been used for the prediction of first hyper-polarizability. The tensor components of the static first hyper-polarizability (β) and second hyper-polarizability (γ) were analytically calculated by using the same method as mentioned above. From the computed tensorial components, β is the calculated for the title compound by taking into account, the Kleinman symmetry relations and the square norm of the Cartesian expression for the β tensor [27]. The relevant expressions used for the calculation are shown below.

$$\beta_{total} = \sqrt{\left(\beta_x^{\,2} + \beta_y^{\,2} + \beta_z^{\,2}\right)}$$

where, $\beta_x = \beta_{xxx} + \beta_{xyy} + \beta_{xzz}$, $\beta_y = \beta_{yyy} + \beta_{xxy} + \beta_{yzz}$, $\beta_z = \beta_{zzz} + \beta_{xxz} + \beta_{yyz}$. The equation for average second hyper-polarizability is

$$\langle\gamma\rangle = \frac{1}{5}\left(\gamma_{xxxx} + \gamma_{yyyy} + \gamma_{zzzz} + 2\gamma_{xxyy} + 2\gamma_{xxzz} + 2\gamma_{yyzz}\right)$$

The calculated values of α, β and γ and the corresponding components are given in Table 1. The calculated second order hyper-polarizability of ATMP is found to be (γ) is $-7.4715\text{x}10^{-30}$ *e.s.u.* The total static dipole moment, polarizabilities, first order hyper-polarizabilities and second order hyper-polarizabilities of ATMP were calculated. Table 1 lists the values of the electric dipole moment (Debye) and dipole moment components, polarizabilities and hyper-polarizabilities (*e.s.u.*) of ATMP. In addition to the

Table 1: Calculated dipole moment, polarizabilities, first order and second order hyperpolarizabilities.

Parameters	Values(a.u.)	
	HF	DFT
μ_x	1.0916	0.7146
μ_y	-0.1897	1.1767
μ_z	-0.8657	-0.4867
μ	1.8770	1.4602
α_{xx}	-71.3427	68.3560
α_{yy}	-76.8587	-66.6131
α_{zz}	-71.0626	-79.1191
α_{xy}	4.2752	-1.4007
α_{xz}	0.5343	1.4438
α_{yz}	1.5348	-1.7044
α_o	-73.088e.s.u	-71.3627e.s.u
$\Delta\alpha$	$2.24\text{x}10^{-37}$e.s.u	$3.13831\text{x}10^{-37}$e.s.u
β_{xxx}	-0.1506	4.3208
β_{yyy}	-5.3271	13.8748
β_{zzz}	-1.6175	-2.0873
β_{xyy}	15.5888	1.8773
β_{xxy}	1.8445	6.7129
β_{xxz}	0.9850	5.6553
β_{xzz}	0.0296	-2.6976
β_{yzz}	2.2550	4.4563
β_{yyz}	-4.2574	10.9264
β_{xyz}	1.7686	-2.5137
β_{tot}	$16.2687\text{x}10^{-31}$e.s.u	$29.1469\text{x}10^{-31}$e.s.u
γ_{xxxx}	-1148.3306	-1212.2583
γ_{yyyy}	-876.5076	-766.7312
γ_{zzzz}	-480.6541	-397.2509
γ_{xxyy}	-337.9411	-329.1180
γ_{xxzz}	-285.2038	-283.0523
γ_{yyzz}	-210.5042	-197.0511
γ	-834.5581	798.9366
	$-7.3398\text{x}10^{-30}$e.s.u	$-7.4715\text{x}10^{-30}$e.s.u

isotropic polarizabilities anisotropy invariant and average second order hyper-polarizability were also calculated. The polarizabilities and first hyper-polarizabilities of ATMP are -72.088, -71.3627 *e.s.u.* and 2.2422, $3.1383\text{x}10^{-37}$*e.s.u.* by HF/6-311+G (d, p) and B3LYP/6-311+G (d, p) levels. The calculated second order hyper-polarizability of ATMP is found to be (γ) is -7.3398 and $-7.4715\text{x}10^{-30}$ *e.s.u.* by HF/6-311+G (d, p) and B3LYP/6-311+G (d, p) levels. According to the magnitude of the first hyper-polarizability, the title compound may be a potential applicant in the development of NLO materials.

3. Results and Discussion

Molecular Geometry

The present compounds under investigation has become a greater interest because it contains two different substituent's namely methyl and amino group. In order to find out the most optimized geometry, the energy calculations were carried out for various possible conformers. The possible four conformer's *cis-cis* (I), *cis-trans* (II), *trans-cis* (III), *trans-trans* (IV) and their corresponding relative energies of ATMP are shown in Fig.1. It is clear from Fig. 1 that the conformer *trans-trans* (IV) have produced the global energy minimum. The most optimized geometrical parameters were calculated for ATMP of *trans-trans* (IV) conformer by B3LYP method with 6-311+G (d, p) basis set. The bond lengths and bond angles are determined from geometrical parameters obtained

from DFT method. The optimized structure can be compared with other similar systems [28] for which the crystal structures have been solved. Therefore optimized geometrical parameters of ATMP are compared with the experimented data of similar kind of molecules [28]. The geometrical parameters obtained from DFT method are seen in good agreement with experimental values of X-ray data [28] and the deviations are due to the presence of amino and methyl groups. Therefore, the experimental X-ray data compared with the DFT method and they are summarized in Table 2. It is known that the six-membered cyclic molecule piperidine and 4-methyl piperidine ring exist in chair forms to can in principle as conformers with NH and NH2 being equatorial (E) and axial (A) [29,30]. Other conformations that differ from the chair (boat, envelope or twist boat) were not considered because of their high energy [29, 30]. It is also known that ATMP is an interesting flexible amino methyl group that can adopt four discrete conformations. The numbering of atoms in ATMP is given in Fig. 2. The calculated structural parameters are presented in Table 2.

Table 2: Optimized geometrical parameters of ATMP bond length(Å), angle(^{0}) and dihedral angle(^{0}) by DFT method

Bond lengths	Value(Å)		Dihedral angles	Value(^{0})
	[a]	Exp[b]		
N1 – C2	1.48	1.51	C6-N1-C2-C3	-51.6
N1 - C6	1.48	1.51	C6-N1-C2-C8	-167.6
N1 - H7	1.02	1.37	C6-N1-C2-C12	73.9
C2 - C3	1.54	1.53	H7-N1-C2-C3	177.2
C2 - C8	1.54	1.54	H7-N1-C2-C8	61.2
C2 - C12	1.55	1.53	H7-N1-C2-C12	-57.4
C3 - C4	1.54	1.53	C2-N1-C6-C5	51.6
C3 - H16	1.10	0.99	C2-N1-C6-C24	167.6
C3 - H17	1.10	0.99	C2-N1-C6-C28	-73.9
C4 - C5	1.54	1.54	H7-N1-C6-C5	-177.2
C4 - N18	1.10	1.46	H7-N1-C6-C24	-61.2
C4 - H19	1.48	1.00	H7-N1-C6-C28	57.4
C5 - C6	1.54	1.53	N1-C2-C3-C4	47.9
C5 - H22	1.10	0.99	N1-C2-C3-H16	172.7
C5 - H23	1.10	0.99	N1-C2-C3-H17	-71.9
C6 - C24	1.54	1.54	C8-C2-C3-C4	162.3
C6 - C28	1.55	1.53	C8-C2-C3-H16	-73.0
C8 - H9	1.09	0.98	C8-C2-C3-H17	42.5
C8 - H10	1.10	0.98	C12-C2-C3-C4	-79.3
C8 - H11	1.09	0.98	C12-C2-C3-H16	45.5
C28 - H29	1.09	0.98	C12-C2-C8-H10	58.9
C28 - H30	1.10	0.98	C12-C2-C8-H11	178.6
C28 - H31	1.10	0.98	N1-C2-C12-H13	53.0
Bond angles	**Value(^{0})**		N1-C2-C12-H14	171.4
	[a]	**Exp[b]**	N1-C2-C12-H15	-68.5
C2 - N1 - C6	121.9	119.6	C3-C2-C12-H13	176.3
C2 - N1 - H7	110.1	117.7	C8-C2-C12-H14	53.7
C6 - N1 - H7	110.1	112.3	C8-C2-C12-H15	173.8
N1 - C2 - C3	107.8	108.6	C2-C3-C4-C5	-48.8
N1 - C2 - C8	106.0	110.1	H16-C3-C4-C5	-173.4
N1 - C2 - C12	114.8	110.8	H17-C3-C4-C5	71.3
C3 - C2 - C8	108.5	105.5	C3-C4-C5-C6	48.8
C3 - C2 - C12	111.9	111.2	C3-C4-C5-H22	-71.3
C8 - C2 - C12	107.6	106.5	C3-C4-C5-H23	173.4
C2 - C3 - C4	115.9	113.1	N18-C4-C5-C6	164.1
C2 - C3 - H16	109.3	109.0	N18-C4-C5-H22	43.9
C2 - C3 - H17	107.7	109.0	N18-C4-C5-H23	-71.4
C4 - 3C - H16	109.8	109.0	N18-C4-H19-H20	-58.8
C4 - C3 - H17	107.0	109.0	N18-C4-H19-H21	58.8
H16 - C3 - H17	106.6	107.8	C4-C5-C6-N1	-47.9
C3 - C4 - C5	110.2	109.6	N1-C6-C28-H29	68.5
C3 - C4 - N18	106.6	110.5	N1-C6-C28-H30	-171.4
C3 - C4 - H19	111.3	107.9	N1-C6-C28-H31	-53.0
C5 - C4 - N18	106.6	112.9		
C5 - C4 - H19	111.3	107.9		
N1 - C6 - C24	106.0	111.7		
N1 - C6 - C28	114.8	111.2		
C5 - C6 - C24	108.5	111.4		
C5 - C6 - C28	111.9	104.2		
C24 - C6 - C28	107.6	109.8		
C2 - C8 - H9	111.0	109.5		
H9 - C8 - H11	109.0	109.5		
H10 - C8 - H11	108.1	109.5		
C2 - C12 - H13	110.0	109.5		
H13 - C12 - H14	107.5	109.5		
C4 - H19 - H20	110.3	-		
C6 - C24 - H25	111.0	109.5		
C6 - C24 - H26	110.6	109.5		
C6 - C24 - H27	110.6	109.5		
H25 - C24 - H26	108.9	109.5		
H25 - C24 - H27	107.5	109.5		
H26 - C24 - H27	108.1	109.5		

[a] Calculated by B3LYP/6311+G(d,p)
[b] S. K. Goswami, L. R. Hanton, C. J. McAdam, S. C. Morattiand J. Simpson , *ActaCryst.* (2011). E67, o3024-o3025

Generally, the C-N-C bond angles are slightly longer and shorter than the C-C-C or N-C-C bond angles [26]. Gundersen and Rankin reported the C-N-C (110.7^0), C-C-C (109.6^0) and N-C-C (110.5^0) bond angles by using electron diffraction technique [28]. In the present study, the bond angles of C-N-C (121.9^0), C-C-C (108.5^0) and N-C-C (107.8^0) by B3LYP method are depicted, in Table 2. The C-N bond lengths are predicted to be slightly shorter than the C-C bond lengths. Gundersen and Rankin [31] reported N-C (1.469 Å) and C-C (1.530 Å) by using electron diffraction technique. In ATMP, the calculated bond length N-C (1.48 Å) and C-C (1.54 Å) by B3LYP/6-311+G (d, p) method have been noticed that the DFT calculations are consistent with the results of electron diffraction data [28]. The ATMP exhibits the chair conformation with computed values of dihedral angles C6-N1-C2-C3, C2-N1-C6-C5, N1-C2-C3-C4, C2-C3-C4-C5, C3-C4-C5-C6 and C4-C5-C6-N1 are -51.6^0, -51.6^0, 47.9^0, -48.8^0, 48.8^0 and -47.9^0 respectively. It can be concluded that the chair form arises due to the van der Waals repulsion between the hydrogen atoms belonging to neighboring carbon atoms.

Vibrational analysis

The ATMP contains 31 atoms, it assuming C_1 symmetry point group. A detailed description of vibrational modes can be given by means of normal coordinate analysis. All vibrations are active both in Raman and infrared absorption. For this purpose, a full set off 107 standard internal coordinates containing 20 redundancies were defined as given in Table 3. From these, a non-redundant set of local symmetry coordinates were constructed by suitable linear combinations of internal coordinates following the recommendations of Pulay et al., and they are presented in Table 4. While both the observed FTIR and FT Raman spectra are rich in bands, there are bonds missing corresponding to the some fundamentals. These fundamentals as well as those corresponding to the observed

bands have been computed at HF and B3LYP levels using the triple split valance basis set along with diffuse and polarization functions, 6-311+G (d, p). The harmonic vibrational frequencies calculated for ATMP at HF and B3LYP levels have been collected in Table5 .All the assignments were subsequently confirmed in the MOLVIB package [17, 18, 32] using HF and B3LYP calculations. .By the help of the calculated potential energy distribution (PED), we assigned the vibrational frequencies of the studied molecule. The calculated frequencies are usually higher than the corresponding experimental quantities, due to the combination of electron correlation effects and basis set deficiencies. After applying the scaling factors, the theoretical calculations reproduce the experimental data well in agreement.

Comparative vibrational frequency analysis

The frequency values computed at HF/6-311+G (d, p) and B3LYP/6-311+G (d, p) basis set contains known systematic error due to negligence of electron correlation. Therefore a linearity can be estimated by plotting the calculated versus experimental frequencies (Fig.3, 4). From the figure 3 and 4, it is found that the calculated (scaled) frequencies by B3LYP with 6-311+G (d, p) basis set are closer to the experimental frequencies than HF method with 6-311+G (d, p) basis set. Certain values obtained by HF and DFT method, are strongly under estimated. If the variations are omitted, the both HF and B3LYP calculations provide good linearity between the calculated and experimental frequencies. The small difference between the experimental and calculated vibrational modes is observed. This discrepancy is from the environment of sample.

Computed IR intensity and Raman activity analysis

Computed vibrational spectral IR intensities and Raman activities of the ATMP molecule for corresponding wave numbers by HF and DFT (B3LYP) methods at 6-311+G (d, p) basis set have been collected in the Table 5. Comparison of IR intensities and Raman activities calculated by HF and DFT (B3LYP) at 6-311+G (d, p) level with experimental values exposes the variation of IR intensities and Raman activities. In most of the cases, the values of IR intensity by HF are found to be higher than B3LYP at 6-311+G (d, p) level

NH2 vibrations

The methylene and amino groups are generally referred to as electron donating substituents in aromatic ring system [33]. The CH2 interacts with nearby π -systems via hyperconjugation, while the NH2 share its lone pair of electrons with the π-electrons in a ring. Both mechanisms imply electronic delocalization is taken into account by the molecular orbital approach. According to Socrates the observed bands 3500-3300 cm^{-1} was assigned to the NH2 stretching modes [34]. The NH2 symmetric and asymmetric vibrations which are assigned to medium strong FTIR band around 3360 cm^{-1} (PED 100%), weak FT Raman band observed at 3310 cm^{-1} (PED 100%) and a medium FTIR around 3288 cm^{-1} (PED 100%), which are very pure mode. Those modes are in good agreement with computed values by HF and B3LYP levels, respectively. The frequencies of amino group appear around 1700-1600 cm^{-1} for scissoring and 1150-900 cm^{-1} for rocking deformations [34]. Hence in the present work, medium strong FTIR bands identified at 1584 cm^{-1} (PED 60%) and 916 cm^{-1} (PED 44%) , both band gives PED contribution to ring and scissoring (CH_2). These vibrations show good agreement with theoretically

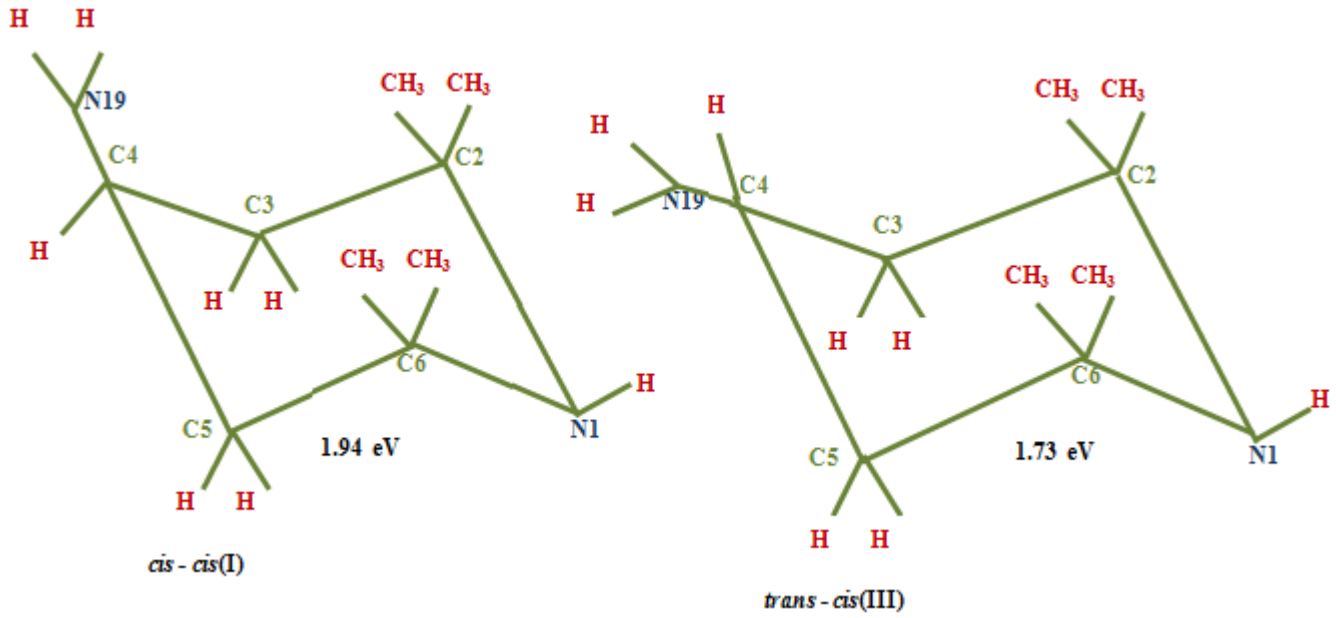

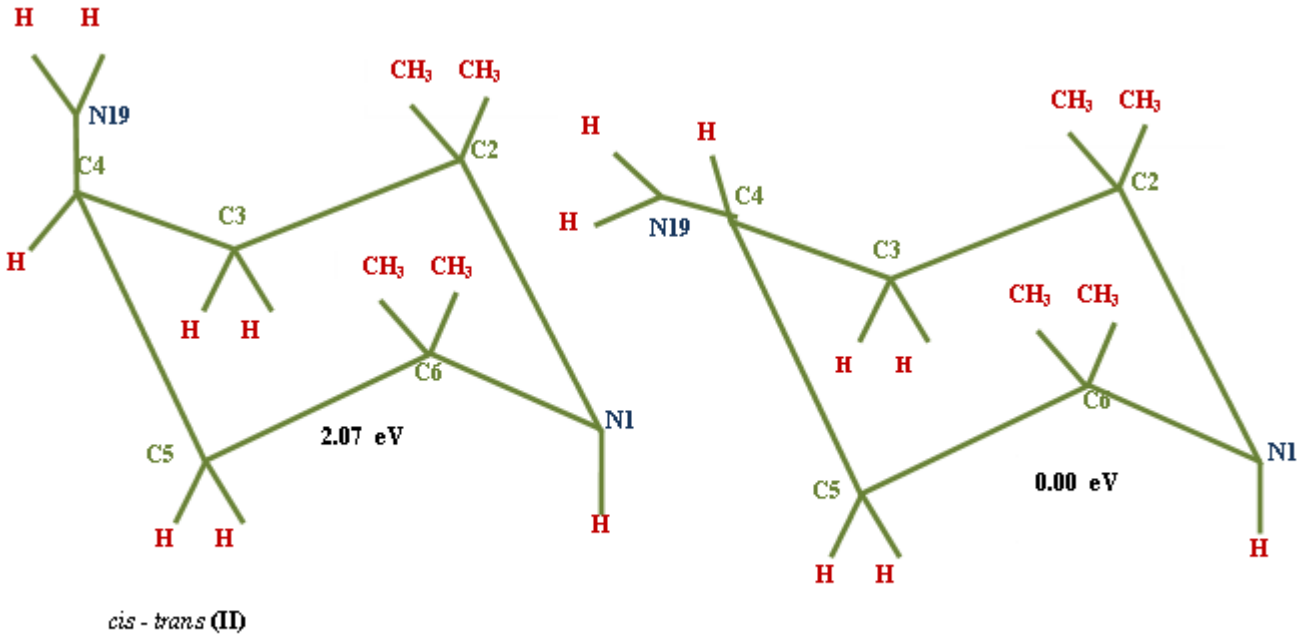

Fig. 1. Possible conformers of ATMP

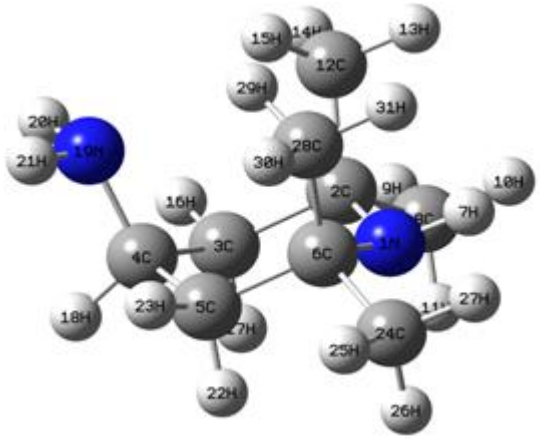

Figure 2: Optimized molecular structure of ATMP

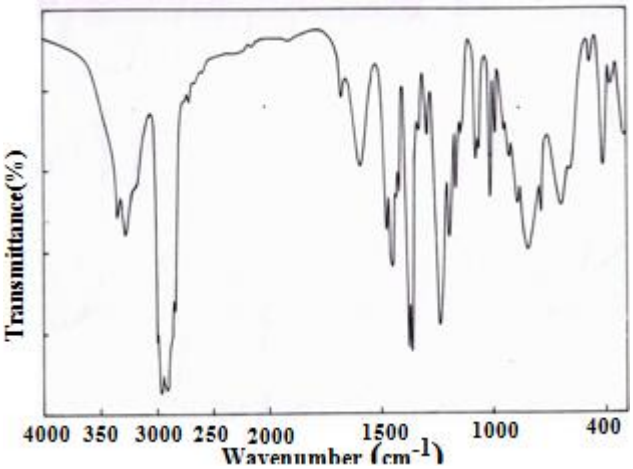

Figure 3: FT-IR spectrum of ATMP

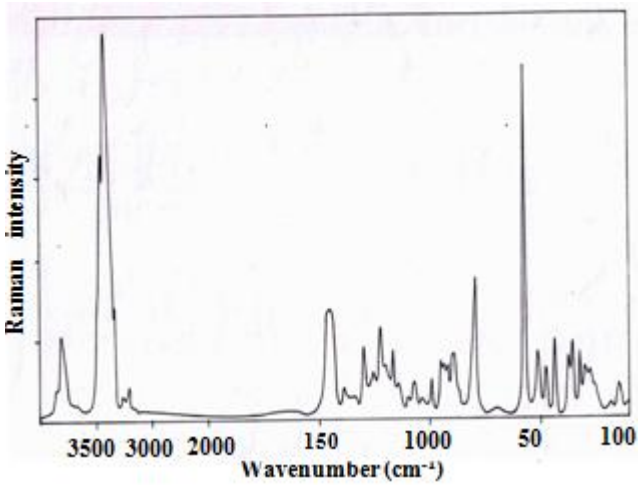

Figure 4: FT-Raman spectrum of ATMP

Table 3: Definition of internal symmetry coordinates of ATMP

No.	*Symbols*	*Type*	*Definition*
		Stretching	
1-3	R_i	N-C	N_1-C_2, N1-C_6
	R_i	N-H	N1-H7
4-7	P_i	C-C	C2 - C3, C2 - C8, C2 - C12, C3 - C4
8-9	Q_i	$C\text{-}H_{(aromatic)}$	C3 - H16, C3 - H17
10	P_i	C-C	C4 - C5
11	R_i	C-N	C4 - N18
12	Q_i	C-H	C4 - H19
13	P_i	C-C	C5 - C6
14-15	Q_i	$C\text{-}H_{(aromatic)}$	C5 - H22, C5 - H23
16-17	P_i	C-C	C6 - C24, C6 - C28
18-23	Q_i	$C\text{-}H_{(me\ 1)}$ $C\text{-}H_{(me\ 2)}$	C8 - H9, C8 - H10, C8 - H11, C12 - H13, C12 - H14, C12 - H15
24-25	R_i	N-H	N19 - H20, N19 - H21
26-31	Q_i	$C\text{-}H_{(me\ 3)}$ $C\text{-}H_{(me\ 4)}$	C24 - H25, C24 - H26, C24 - H27 C28 - H29, C28 - H30, C28 - H31
		In-plane bending	

32	β_i	$CNC_{(ring)}$	C2 - N1 - C6
33-34	α_i	CNH	C2 - N1 - H7,C6 - N1 - H7
35 36-37	β_i α_i	$NCC_{(ring)}$ NCC	N1 - C2 - C3 N1 - C2 - C8, N1 - C2 - C12
38-39 40-41	α_i β_i	CCC $CCC_{(ring)}$	C3 - C2 - C8,C3 - C2 - C12 C8 - C2 - C12,C2 - C3 - C4
42-46	α_i	$CCH_{(aromatic)}$	C2 - C3 - H16,C2 -C3 -H17,C4 - 3C -H16,C4 - C3 -H17, H16 -C3 - H17,
47	β_i	$CCC_{(ring)}$	C3 - C4 - C5
48-52	α_i	CCH, CCN	C3 -C4 -H18,C3 -C4 -N19,C5 - C4 - H18,C5 -C4 - N19,H18 -C4 -N19
53	β_i	$CCC_{(ring)}$	C4 - C5 - C6
54-58	α_i	$CCH_{(aromatic)}$	C4 -C5 -H22,C4 - C5 - H23,C6 - C5-H22,C6 -C5 - H23,H22 -C5 - H23
59	β_i	$NCC_{(ring)}$	N1 - C6 - C5
60-64	α_i	NCC	N1 -C6 -C24,N1 -C6 -C28,C5 - C6 - C24,C5-C6 -C28,C24 -C6 - C28
65-67	α_i	$CCH_{3(me\ 1)}$ HCH	C2 - C8 - H9,C2 - C8 - H10,C2 - C8 - H11
68-70	α_i		H9 - C8 - H10, H9 - C8 - H11,H10 - C8 - H11
71-73	α_i	$CCH_{3(me\ 2)}$ HCH	C2 - C12 - H13,C2 - C12 - H14, C2 - C12 - H15
74-76	β_i		H13 - C12 - H14,H13 - C12 - H15, H14 - C12 - H15
77-79	β_i	$NH_{2(aromatic)}$	C4 - N19 - H20,C4 - N19 - H21, H20-N19-H21
80-82	β_i	$CCH_{3(me\ 3)}$ HCH	C6 - C24 - H25, C6 - C24 - H26, C6 - C24 - H27
83-85	β_i		H25 - C24 - H26, H25 - C24 - H27, H26 - C24 - H27
86-88	β_i	$CCH_{3(me\ 4)}$	C6 - C28 - H29, C6 - C28 - H30,C6 - C28 - H31
89-91	β_i	HCH	H29 - C28 - H30,H29 - C28 - H31, H30 - C28 - H31
92-93		CNH	C4-N1-H21, C4-N1-H20
Out-of-plane bending			
94-95	τ_i	$C(CH_3)_{2(1)}$	(C6,H7)N1-C2-C3(C8, C12), (C2, H7)-N1-C6-(C5, C24, C28)
96	τ_i	$CH_{2(1)}$	(N1, C8,C12)-C2-C3-(C4, H16, H17)
97	τ_i	$CH_{3(1)}$	(N1, C3, C12)-C2-C8-(H9, H10, H11)
98	τ_i	$CH_{3(2)}$	(N1, C3, C8)- C2-C12-(H13, H14, H15)
99	τ_i	CNH	(C2, H16, H17)- C3-C4-(C5, H18, N19)
100	τ_i	NH_2	(C3, C5, H18)-C4-N19-(H20, H21)
101	τ_i	$C(CH_3)_{2\ (2)}$	(C4, H22, H23)-C5-C6-(N1, C24, C28)
102	τ_i	$CH_{3(3)}$	(N1, C5, C28)-C6-C24-(H25, H26, H27)
103	τ_i	$CH_{3(4)}$	(N1, C5, C24)-C6-C28-(H29, H30, H31)
104-109	τ_i	Ring	C6-N1-C2-C3, N1-C2-C3-C4, C2-C3-C4-C5, C3-C4-C5-C6, C4-C5-C6-N1, C5-C6-N1-C2

Table 4: Definition of local symmetry coordinates of ATMP

No.	Type	Definition
Stretching		
1-3	C-N	R_1, R_2, R_{11}
4-11	C-C	Q_4, Q_5, Q_6, Q_7, Q_{10}, Q_{13}, Q_{16}, Q_{17}
12	N-H	R_3
13-17	CH	R_8, R_9, R_{12}, R_{14}, R_{15}
18-20	$CH_{3(me\ 1)}$	$(Q_{18}+Q_{19}+Q_{20})/\sqrt{3}$, $(Q_{18}-Q_{19}-Q_{20})/\sqrt{6}$, $(Q_{19}-Q_{20})/\sqrt{2}$
21-23	$CH_{3(me\ 2)}$	$(Q_{21}+Q_{22}+Q_{23})/\sqrt{3}$, $(Q_{21}-Q_{22}-Q_{23})/\sqrt{6}$, $(Q_{22}-Q_{23})/\sqrt{2}$
24	NH_2ss	$(R_{24}+R_{25})/\sqrt{2}$
25	NH_2ass	$(R_{24}-R_{25})/\sqrt{2}$
26-28	$CH_{3(me\ 3)}$	$(Q_{26}+Q_{27}+Q_{28})/\sqrt{3}$, $(Q_{26}-Q_{27}-Q_{28})/\sqrt{6}$, $(Q_{27}-Q_{28})/\sqrt{2}$
29-31	$CH_{3(me\ 4)}$	$(Q_{29}+Q_{30}+Q_{31})/\sqrt{3}$, $(Q_{29}-Q_{30}-Q_{31})/\sqrt{6}$, $(Q_{30}-Q_{31})/\sqrt{2}$
In-plane bending		
32	CNH	$(\alpha_{33}-\alpha_{34})\ \sqrt{6}$
33	$C-(CH_3)_2$	$\alpha_{36}+\alpha_{37}+\alpha_{38}+\alpha_{39}$, $\alpha_{36}-\alpha_{37}+\alpha_{38}-\alpha_{39}$, $\alpha_{36}+\alpha_{37}-\alpha_{38}-\alpha_{39}$
36	$CH_2(1)$	$\alpha_{42}+\alpha_{43}+\alpha_{44}+\alpha_{45}$, $\alpha_{42}-\alpha_{43}+\alpha_{44}-\alpha_{45}$, $\alpha_{42}+\alpha_{43}-\alpha_{44}-\alpha_{45}$
39	CCN, CCH	$\alpha_{48}+\alpha_{49}+\alpha_{50}+\alpha_{51}$, $\alpha_{48}-\alpha_{49}+\alpha_{50}-\alpha_{51}$, $\alpha_{48}+\alpha_{49}-\alpha_{50}-\alpha_{51}$
42	$CH_2(2)$	$\alpha_{54}+\alpha_{55}+\alpha_{56}+\alpha_{57}$, $\alpha_{54}-\alpha_{55}+\alpha_{56}-\alpha_{57}$, $\alpha_{54}+\alpha_{55}-\alpha_{56}-\alpha_{57}$
45	$C-(CH_3)_2$	$\alpha_{60}+\alpha_{61}+\alpha_{62}+\alpha_{63}$, $\alpha_{60}-\alpha_{61}+\alpha_{62}-\alpha_{63}$, $\alpha_{60}+\alpha_{61}-\alpha_{62}-\alpha_{63}$
48	$(C-CH_3)_{Sb}$	$(-\alpha_{65}-\alpha_{66}-\alpha_{67}+\alpha_{68}+\alpha_{69}+\alpha_{70})/\sqrt{6}$
49	CH_{3ipb}	$(-\alpha_{68}-2\alpha_{69}-\alpha_{70})/\sqrt{6}$
50	CH_{3opb}	$(-\alpha_{68}-\alpha_{70})/\sqrt{6}$
51	CH_{3ipr}	$(-\alpha_{65}+2\alpha_{66}-\alpha_{67})/\sqrt{6}$
52	CH_{3opr}	$(\alpha_{65}-\alpha_{67})/\sqrt{6}$
53	$(C-CH_3)_{Sb}$	$(-\alpha_{71}-\alpha_{72}-\alpha_{73}+\alpha_{74}+\alpha_{75}+\alpha_{76})/\sqrt{6}$
54	CH_{3ipb}	$(-\alpha_{74}-2\alpha_{75}-\alpha_{76})/\sqrt{6}$
55	CH_{3opb}	$(-\alpha_{74}-\alpha_{76})/\sqrt{6}$
56	CH_{3ipr}	$(-\alpha_{71}+2\alpha_{72}-\alpha_{73})/\sqrt{6}$
57	CH_{3opr}	$(\alpha_{71}-\alpha_{73})/\sqrt{6}$
58	NH_{2rock}	$(\alpha_{77}-\alpha_{78})/\sqrt{2}$
59	NH_{2wag}	$(\alpha_{77}+\alpha_{78})/\sqrt{2}$
60	NH_{2sciss}	$(2\alpha_{79}-\alpha_{77}-\alpha_{78})/\sqrt{6}$
61	$C-CH_{3\ Sb}$	$(-\alpha_{80}-\alpha_{81}-\alpha_{82}+\alpha_{83}+\alpha_{84}+\alpha_{85})/\sqrt{6}$
62	CH_{3ipb}	$(-\alpha_{83}-2\alpha_{84}-\alpha_{85})/\sqrt{6}$
63	CH_{3opb}	$(-\alpha_{83}-\alpha_{85})/\sqrt{6}$
64	CH_{3ipr}	$(-\alpha_{80}+2\alpha_{81}-\alpha_{82})/\sqrt{6}$
65	CH_{3opr}	$(\alpha_{80}-\alpha_{82})/\sqrt{6}$
66	$C-CH_{3\ Sb}$	$(-\alpha_{86}-\alpha_{87}-\alpha_{88}+\alpha_{89}+\alpha_{90}+\alpha_{91})/\sqrt{6}$
67	CH_{3ipb}	$(-\alpha_{89}-2\alpha_{90}-\alpha_{91})/\sqrt{6}$
68	CH_{3opb}	$(-\alpha_{89}-\alpha_{90})/\sqrt{6}$
69	CH_{3ipr}	$(-\alpha_{86}+2\alpha_{87}-\alpha_{88})/\sqrt{6}$
70	CH_{3opr}	$(\alpha_{86}-\alpha_{88})/\sqrt{6}$
71	R_{trigd}	$(\beta_{32}-\beta_{35}+\beta_{41}-\beta_{47}+\beta_{53}-\beta_{59})/\sqrt{6}$
72	R_{symd}	$(-\beta_{32}-\beta_{35}+\beta_{41}-\beta_{47}-\beta_{53}+\beta_{59})/\sqrt{12}$
73	R_{assymd}	$(\beta_{32}-\beta_{35}+\beta_{41}-\beta_{47})/2$
74		$(\alpha_{92}-\alpha_{93})/\sqrt{6}$
Out-of-plane bending		
75-77	$CC_2(1)$	τ_{94}, τ_{95}, τ_{9101}
78	$CH_2(1)$	τ_{96},
79-82	$CH_3(1)$	τ_{97}, τ_{98}, τ_{102}, τ_{103}
83	CNH	τ_{99}
84	NH_2	τ_{100}
85	τ_{Rtrigd}	$(\tau_{104}-\tau_{105}+\tau_{106}-\tau_{107}+\tau_{108}-\tau_{109})/\sqrt{6}$
86	τ_{Rsymd}	$(\tau_{104}-\tau_{105}+\tau_{108}-\tau_{109})/2$
87	$\tau_{Rassymd}$	$(-\tau_{104}-\tau_{105}-\tau_{106}-\tau_{107}+\tau_{108}-\tau_{109})/\sqrt{12}$

The title molecule ATMP under consideration possesses four CH_3 groups. These are split in to two CH_3 group are in second position of piperidine ring and two CH_3 group are in 6 position of piperidine ring. The important vibrational modes of this moiety is (C-$(CH_3)_2$ stretching and methyl deformation. Methyl groups are generally referred to as electron donating substituents in the aromatic ring system [35,36]. Absorption arising from C-H stretching in methyl group lies in the region 3000 - 2840 cm^{-1}. Normally the asymmetric stretching vibrations (ν CH_3ass) are found at 2962 cm^{-1} and that of symmetric stretching vibrations at 2873 cm^{-1} [37, 38]. Here the CH_3 symmetric stretching bands appear at 2851 cm^{-1} and that of asymmetric as 2920 cm^{-1}(PED 94%) in FT Raman. The lowering of the wavenumbers from the normal values is due to the intramolecular charge transfer (ICT) from thetetramethyl group to the aromatic ring. The change in intensity of the CH_3 stretching mode is also due to the influence of electronic effects resulting from hyperconjugation of methyl group and aromatic ring system. This can point to change in polarizability and dipolemoment due to electron delocalization. Thus the hyperconjugation of methyl group, causing changes in intensity in Raman, clearly indicates that methyl hydrogen is directly involved in the donation of electronic charge. Of CH_3 deformation frequencies [38,39], there are four asymmetric bending vibrations observed in the region 1470-1420 cm^{-1} and a symmetric bending vibration near 1360 cm^{-1}. Hence, in the present investigation, the weak FT Raman band at 1480 cm^{-1}(PED%) and medium strong FTIR band at 1430 cm^{-1} (PED%) have been assigned to asymmetric and symmetric deformation with major contribution to ν(CC) of CH_3group. The relatively large value of IR and Raman intensity of the asymmetric and symmetric bending mode suggests a large positive charge localized on hydrogen, which further supports the presence of hyper conjugation [39]. These fundamentals are good agreement with the calculated values at 1499, 1470, 1459 cm^{-1} and 1463, 1450, 1444 cm^{-1} by HF/ 6-311+G (d, p) and B3LYP/6-311+G (d, p) methods, respectively. The rocking modes of the CH_3 groups are expected to appear in the region 1070-1010 cm^{-1}.The very intense band at 1156, 1096, 1076 cm^{-1} (Raman) and 1168, 1136, 1097 cm^{-1}(IR) are assigned to CH_3 rocking modes in ATMP. The relatively large value of intensity in IR and Raman wavenumbers of the rocking modes suggests the presence of hyperconjugation. The scissoring and torsion vibrations are identified below 800 cm^{-1}which is supported by the computed wavenumbers. The C-N stretching modes and other structural modes have also been identified.

Ethyl(cyclohexane) vibration

The CH_2 interacts with nearby π –systems via hyperconjugation, while the NH_2 share its lone pair of electrons with the π-electrons in a ring. This mechanism implies electronic delocalization is taken into account by the molecular orbital approach. The CH_2 group gives rise to six internal modes of vibrations such as the asymmetric stretching, symmetric stretching, the symmetric planar deformation or scissoring, the antisymmetric planar deformation or rocking, the symmetric non-planar deformation or wagging and the anti-symmetric non-planar deformation or torsion. The molecule under investigation possesses two CH_2 group and hence one can expect two symmetric and two asymmetric C-H stretching vibrations. It is stated that in cyclohexane, the C-H stretching vibrations occur in the region 3000-2800 cm^{-1}. The asymmetric –CH_2 stretching vibration appears from 3000 to 2900 cm^{-1} and the symmetric –CH_2 stretching is observed in the range 2900-2800 cm^{-1} [40].

The antisymmetric stretching mode is calculated at the wavenumber 2883, 2882 cm^{-1} than the symmetric one at 2881, 2880 cm^{-1} by HF/ 6-311+G (d, p) and B3LYP/6-311+G (d, p) methods respectively. The deformation mode of the CH2 group appears in the region around 1470 cm^{-1} [41]. The calculated frequency for the scissoring mode of CH2 is 1458, 1448 and 1443, 1428 cm^{-1} by HF/ 6-311+G (d, p) and B3LYP/6-311+G (d, p) methods, respectively. This mode is also coupled with ring stretching mode as shown in Table 5. The observed medium strong band at 1192 cm^{-1} in IR spectrum is attributed to the appreciable contribution from the C-H in plane bending suggests its origin due to the wagging mode. The theoretically predicted frequency by HF/ 6-311+G (d, p) and B3LYP/6-311+G (d, p) methods, respectively at 861, 889 and 889, 814 cm^{-1}.

C-C and C-N vibrations

Most of the ring vibrational modes are affected by the substitutions in the ring of the title molecule. The characteristic ring stretching vibrations are assigned in the region 1650-1300 cm^{-1} [42, 43]. The C-C stretching vibrations of ATMP are found in the range 1360 cm^{-1} and 1240 cm^{-1} in Raman spectrum. The theoretically computed values for C-C vibrational modes by HF/ 6-311+G (d, p) and B3LYP/6-311+G (d, p) methods give excellent agreement with the experimental data. The C-C in plane bending vibrations are assigned in the region ~550-300 cm^{-1}. On account of the heavy substitution on the ring these vibrations have shifted to lower frequencies from their usual range, making assignment difficult. In ATMP, the medium FT Raman band observed at 317, 294, 274 cm^{-1}(PED %) without corresponding FTIR band is assigned to C-C in plane bending vibration. The weak FTIR band at 424 cm^{-1} and very weak FT Raman band identified at 432 cm^{-1} for ATMP have been assigned to ring out-of-plane vibrations. The scaled values by HF/ 6-311+G (d, p) and B3LYP/6-311+G (d, p) methods predict at 460, 444, 389 and 455, 421, 396 cm^{-1} are show good agreement with experimentally recorded spectra.Weak to medium intensity bands for unconjugated C-N bond in primary, secondary and tertiary aliphatic amines occur in the region of 1000-1250 cm^{-1}. They are due to coupled C-N stretching modes. The position of the bands in this region depends on the nature of the amine and the pattern of substitution on the α-carbon atom. Aromatic amines show strong C-N stretching bands at higher frequencies, 1260-1340 cm^{-1} than the corresponding bands of aliphatic amines since the C-N bond order is increased due to conjugation with the ring [44]. Hence, in the present investigation, the FTIR band at 1264 and 1260 cm^{-1} (PED %) have been assigned to C-N stretching modes. These fundamentals are good agreement with the calculated values at 1254, 1240 cm^{-1} and 1235, 1220 cm^{-1} by HF/ 6-311+G (d, p) and B3LYP/6-311+G (d, p) methods, respectively.

4. Other molecular properties

Natural bond orbital analysis

The Natural Bond Orbital (NBO) calculation was performed using NBO 3.1 program implemented in the Gaussian 09W [11] package at the DFT/B3LYP6-311+G (d, p)) level of theory. NBO analysis transforms the calculated canonical delocalized DFT molecular orbitals (MOs) into localized molecular orbitals (MOs) that are closely tied to chemical bonding concepts. This process involves sequential transform of non-orthogonal atomic orbital's (AO's) to the sets of natural atomic orbital's (NAOs), natural hybrid orbital's (NHOs) and natural bond orbital's (NBOs). The localized basis set completely describes the wave functions in the most economic method, as electron density and other properties that are described by the minimal amount of filled NBO's. This non-covalent bonding and antibonding charge transfer interactions can be quantitatively described in terms of the second order perturbation interaction energy ($E^{(2)}$) [45,46].This energy represents the estimate of the off diagonal NBO Fock matrix elements. It can be deduced from the second-order perturbation approach [47] as follows:

$$E^{(2)} = -n_\sigma \frac{\langle \sigma|F|\sigma\rangle^2}{\varepsilon\sigma^* - \varepsilon_\sigma} = -n_\sigma \frac{F_{ij}^2}{\Delta E}$$

where $\langle \sigma|F|\sigma\rangle^2$, or F_{ij}^2 is the Fock matrix elements between i and j NBO orbital, ε_σ and $\varepsilon\sigma^*$ are the energies (diagonal elements) of σ and σ^* NBO's, and n_σ is the population of the donor σ obtained occupancy.

Delocalization of the electron density (ED) between occupied Lewis type (bond (or) lone pair) NBO orbitals and formally unoccupied (antibond (or) Rydberg) non-Lewis NBO orbitals corresponds to a stabilizing donor-acceptor interaction. The corresponding results have been tabulated in Table 6. The NBO analysis also describes the bonding in terms of the natural hybrid occupancy (number of electron (or) "natural population" of the orbital). It is noted that the maximum energy occupancies 1.9872, 1.9798, 1.9796, 1.9795 electrons are obtained to BD(C_4-N_{19}), BD(N_1-C_6), BD(N_1-H_7), BD(C_6-C_{24}), respectively. The *sp* compositions with considerable *p*-characters 78.22%, 69.49%, 77.70%, 74.46% are also tabulated in Table 6. Therefore, the results suggest that the C_4-N_{19}, N_1-C_6, N_1-H_7, C_6-C_{24}, bond lengths 1.48, 1.48, 1.02, 1.54 of ATMP are essentially controlled by the *p* -character of these hybrid orbital's.

Table 7: The second order perturbation energies E (2) (kcal /mol) corresponding to the most important charge transfer interactions (donor −acceptor) of ATMP by DFT method.

Donor NBO (i)	Acceptor NBO (j)	E(2)[a] kcal/mol	E(j)—E(i)[b] a.u.	F(i,j)[c] a.u.
LP (N1)	BD*(C2 - C12)	7.17	0.67	0.063
LP (N1)	BD*(C6 - C24)	6.84	0.66	0.061
LP (N19)	BD*(C2 - C3)	2.94	0.64	0.039
LP (N19)	BD*(C3 - C4)	3.4	0.61	0.041
LP (N19)	BD*(C4 - H18)	1.57	0.6	0.028

Table 5: Vibrational assignments, infrared intensities, Raman activities and Raman intensity of ATMP based on HF and B3LYP/6-311+G**

Observed frequencies cm^{-1}		Calculated frequencies cm^{-1}				Reduced mass (amu)		Force constant (mdyneA^{-1})		IR intensity (km)mol^{-1}		Raman activity A^0(amu)		Raman intensity (km)mol^{-1}		Assignments/ (%PED)
FTIR	FT−Raman	Unscaled		Scaled												
		a	b	a	b	a	b	a	b	a	b	a	b	a	b	
3360(ms)		3855	3562	3370	3353	1.09	1.09	8.17	9.52	0.05	2.61	71.55	25.43	6.86	4.02	ν NH2 ass(100)
	3310(w)	3777	3512	3292	3306	1.07	1.08	7.80	9.04	0.93	1.06	83.81	46.02	8.41	7.61	ν NHss(100)
3288(ms)		3751	3485	3269	3280	1.05	1.06	7.51	8.75	1.06	0.26	157.00	104.41	16.2	17.70	ν NH2 ss(100)
3000(vs)		3301	3157	2962	2960	1.09	1.09	6.42	7.00	7.30	49.05	39.33	47.97	5.50	11.05	ν CH3ass(99)
		3272	3141	2946	2952	1.10	1.10	6.37	6.91	7.47	50.44	37.29	35.63	5.25	8.27	ν CH3ass(99)
	2920(s)	3239	3103	2906	2920	1.10	1.10	6.25	6.81	44.43	95.18	124.18	165.23	18.0	39.55	ν CH3ass(96)
		3236	3102	2899	2916	1.10	1.10	6.24	6.80	18.28	56.07	1.77	78.41	0.26	18.84	ν CH3ass(94)
		3228	3078	2892	2893	1.10	1.10	6.14	6.77	85.82	1.75	189.79	11.46	28.3	2.82	ν CH3ass(93)
		3226	3077	2890	2892	1.10	1.10	6.14	6.76	39.58	4.03	39.21	8.43	5.85	2.07	ν CH3ass(94)
		3218	3065	2883	2881	1.10	1.10	6.10	6.70	20.42	76.22	58.37	161.77	8.80	40.20	ν CH2 ass(94)
		3216	3064	2882	2880	1.10	1.10	6.09	6.70	22.72	54.67	32.53	26.33	4.91	6.55	ν CH2 ass(93)
		3208	3057	2874	2873	1.10	1.10	6.07	6.65	36.43	8.71	53.94	27.71	8.20	6.94	ν CH3 ss (96)+ CH2 SS
		3181	3054	2855	2870	1.10	1.07	6.06	6.39	5.11	43.93	17.33	398.15	2.64	100.0	ν CH3 ss (89)+ CH2 SS
	2851(vs)	3179	3026	2852	2848	1.05	1.08	5.69	6.44	1.52	52.30	642.36	135.16	100.0	34.67	ν CH3 ss (94)+ CH2 SS
		3176	3021	2846	2839	1.05	1.06	5.63	6.29	115.1	75.66	6.65	28.26	1.04	7.31	ν CH3 ss (94)+ CH2 SS (42)
		3172	3017	2842	2836	1.05	1.06	5.61	6.30	70.59	28.31	106.23	28.75	16.7	7.46	ν CH3 ss (91)+ CH2 SS(43)
		3157	3015	2829	2834	1.05	1.04	5.62	6.13	0.11	47.58	24.71	97.27	3.90	25.29	ν CH3 ss (93)+ CH2 SS (55)
		3156	3013	2828	2832	1.04	1.04	5.56	6.10	35.63	31.86	8.93	65.44	1.41	17.05	ν CH2 ss (95)+ CH2 SS (45)
		3146	3011	2819	2830	1.04	1.07	5.56	6.21	1.79	3.33	17.55	16.80	2.78	4.38	ν CH2 ss (93)+ CH2 SS(43)
	2759(vw)	3138	2927	2812	2755	1.08	1.06	5.47	6.17	74.64	14.68	129.90	26.18	22.1	7.35	ν CH(99)
1584(ms)		1801	1654	1614	1584	1.09	1.10	1.76	2.11	43.04	38.38	3.58	2.38	2.03	2.22	NH2 sci(60)+CH2 sci(30)
	1480(w)	1673	1528	1499	1463	1.06	1.23	1.46	2.03	18.80	15.48	1.93	0.69	1.26	0.74	CH3ad(61)
		1641	1527	1470	1450	1.19	1.06	1.64	1.68	10.66	8.91	1.56	0.17	1.04	0.19	CH3 ad(57)

		1627	1504	1458	1444	1.05	1.06	1.40	1.65	0.87	8.77	11.61	1.80	7.76	1.98	CH3 ad(65)
		1627	1503	1458	1443	1.06	1.07	1.41	1.67	2.36	1.22	2.67	7.69	1.79	8.48	CH2 sci(74)+ν ring (40)
		1616	1491	1448	1428	1.06	1.08	1.39	1.66	15.61	9.69	2.62	1.71	1.78	1.92	CH2 sci(71)+ν ring (33)
1444(s)		1615	1487	1447	1427	1.05	1.07	1.37	1.64	1.10	1.72	6.19	10.56	4.22	11.87	CH3opr(51)
		1612	1487	1444	1427	1.06	1.05	1.38	1.61	3.32	1.58	3.82	12.95	2.61	14.56	CH3opr(65)
		1605	1482	1438	1423	1.11	1.05	1.44	1.60	0.23	1.89	3.90	1.36	2.67	1.54	CH3opr(58)
1430(ms)		1602	1478	1435	1419	1.08	1.08	1.38	1.63	0.31	0.29	0.95	0.29	0.65	0.33	CH3sd(78)
1430(ms)		1599	1472	1433	1413	1.07	1.07	1.37	1.61	6.50	5.22	16.08	8.52	11.1	9.74	CH3sd(67)
		1590	1467	1425	1405	1.09	1.08	1.38	1.61	8.67	2.81	2.44	3.33	1.71	3.84	CH3sd(48)
		1560	1420	1398	1360	1.25	1.30	1.48	1.86	8.22	9.04	1.04	3.69	0.77	4.50	CH3sd(77)
		1548	1411	1387	1354	1.33	1.26	1.56	1.77	29.82	6.81	1.46	0.99	1.09	1.22	CH3opr(70)
1360(vs)		1539	1403	1381	1344	1.44	1.24	1.67	1.73	0.27	19.93	0.72	1.10	0.54	1.37	*ν CC(55)*
		1531	1402	1372	1343	1.31	1.38	1.51	1.91	1.06	15.52	0.66	1.13	0.50	1.41	C-CH3 opd (60)
		1521	1392	1363	1333	1.23	1.27	1.40	1.73	30.29	1.07	0.33	0.11	0.25	0.14	C-CH3 opd(57)
		1515	1386	1357	1328	1.25	1.52	1.41	2.06	0.05	4.82	0.09	2.13	0.07	2.70	C-CH3 opd(61)
	1312(vw)	1502	1379	1347	1321	1.69	1.39	1.89	1.85	18.95	0.72	1.88	0.72	1.46	0.92	C-CH3opd(58)
	1312(vw)	1456	1361	1306	1303	1.46	1.48	1.60	1.85	1.31	1.89	1.50	3.97	1.19	5.20	*CH2 twist* (48)
1295(ms)		1450	1322	1301	1267	1.23	1.64	1.26	2.04	3.54	10.26	5.42	6.35	4.51	8.71	*CH2 twist(52)*
	1264(vw)	1398	1290	1254	1235	2.87	2.03	2.82	2.33	10.54	64.87	11.16	1.35	9.69	1.93	ν CN(55)
	1240(w)	1382	1274	1240	1220	1.77	2.54	1.69	2.86	39.39	34.54	1.09	9.41	0.97	13.73	ν CN(58)
1213		1358	1239	1241	1228	1.75	2.60	1.58	2.83	5.00	20.66	5.73	8.13	5.02	11.74	NH2 wag(45)
1192(ms)	1204(vw)	1332	1218	1217	1207	2.84	2.44	2.48	2.55	1.40	3.71	1.04	2.29	0.94	3.40	CH2 wag (48) + CH ipd (28)
	1180(w)	1327	1200	1213	1189	2.78	2.45	2.35	2.55	42.42	1.03	15.73	1.76	14.5	2.68	CH2 wag (38)
1168(ms)		1270	1191	1199	1180	1.87	1.89	1.57	1.79	0.00	3.12	2.42	3.25	2.26	5.00	CH3ipr (45)
1136(w)	1156(vw)	1253	1159	1183	1149	1.60	1.30	1.27	1.21	42.60	23.20	5.66	5.81	5.52	9.33	CH3ipr (61)
1097(ms)	1096(vw)	1220	1120	1152	1110	1.59	1.60	1.17	1.41	4.69	6.47	2.76	3.35	2.84	5.68	CH3ipr (57)
1054(w)	1072(vw)	1180	1076	1114	1067	1.79	1.69	1.22	1.38	4.07	4.02	4.60	7.25	5.03	13.07	CH3ipr (63)
	1036(vw)	1160	1042	1095	1033	1.76	1.69	1.13	1.34	0.00	13.23	5.01	6.37	5.76	12.07	ν CN(62)
1012(ms)		1127	1032	1062	1023	1.78	2.04	1.12	1.52	6.73	11.18	1.32	0.23	1.54	0.44	ν CC(61)
1000(w)		1109	1024	1047	1015	1.44	1.41	0.89	1.02	1.21	2.21	1.22	0.83	1.44	1.61	ν CC(62)
		1104	1013	1042	1004	1.44	1.36	0.87	0.97	0.68	0.64	0.61	0.81	0.73	1.60	CH3 ipd(33)
	990(vw)	1075	1001	1015	992	1.71	1.88	1.01	1.28	5.21	2.82	3.70	3.76	4.52	7.57	ν CC(85)
	945(w)	1017	960	960	952	2.11	1.49	1.14	0.91	4.73	1.31	2.79	1.93	3.63	4.14	ν CC(88)
916(w)	922(w)	1011	933	955	925	1.48	1.63	0.76	0.98	7.82	2.30	3.93	8.07	5.34	18.05	NH2 rock(44) +ring(25)
	922(w)	1007	923	950	915	1.48	1.48	0.75	0.88	0.64	0.07	6.13	6.76	8.46	15.37	Ring(30)
892(ms)	899(w)	981	909	926	901	2.25	2.12	1.10	1.20	0.69	2.94	0.62	6.87	0.88	15.98	Ring(32)
		979	906	877	898	1.73	1.93	0.84	1.09	24.14	6.90	11.85	0.60	16.8	1.40	b CNH(42)
		961	897	861	889	2.20	2.00	1.04	1.09	1.83	12.47	2.96	0.73	4.26	1.73	CH2 rock(75)
		920	882	824	874	1.77	1.54	0.81	0.77	0.00	88.46	1.52	1.50	2.24	3.65	CH2 rock(75)
823		884	840	814	798	1.80	2.17	0.75	1.00	44.48	52.10	1.29	2.75	2.18	7.64	Ring(32)
770	785(ms)	849	784	801	777	2.89	3.22	1.05	1.37	41.76	2.68	4.53	6.24	7.94	18.03	twist CH3(80)
		811	765	766	700	3.10	2.97	1.07	1.15	0.40	0.31	0.45	0.61	0.92	2.05	b CCC(61)
660	705(vw)	782	677	738	705	1.86	1.80	0.50	0.65	52.34	77.64	2.68	5.30	5.41	17.63	twist CH3(85)
633	580(vs)	669	649	632	594	3.78	3.34	0.94	0.88	13.73	7.76	20.34	19.65	52.54	83.64	twist CH3 (81)
	523(w)	564	537	533	532	2.96	2.83	0.50	0.53	4.32	1.84	6.84	3.86	20.72	19.27	twist CH3(66)
505		562	520	530	515	2.83	2.87	0.45	0.53	4.62	6.64	1.49	3.16	4.73	16.54	twist CNH(63)
464	477(vw)	505	467	477	463	1.70	1.71	0.22	0.26	21.29	15.99	0.25	0.41	0.93	2.51	ν CH(81)
		499	459	460	455	2.14	2.23	0.27	0.33	0.00	0.92	0.10	0.16	0.38	1.00	γ CCC ring(67)
424(w)	432(vw)	470	425	444	421	2.10	2.05	0.22	0.27	0.22	6.35	0.05	0.06	0.21	0.42	γ CCC ring(65)
		434	400	389	396	1.90	1.92	0.18	0.21	0.55	0.06	0.21	0.52	0.98	4.02	γ CCC ring(61)
	374(w)	381	357	360	374	2.39	2.67	0.18	0.23	1.03	0.33	1.75	2.10	8.94	17.69	C-CH3 sci(45)
	352(w)	376	353	355	349	2.97	2.89	0.22	0.24	3.03	3.11	1.61	1.60	9.15	14.98	b CNC(41)
	317(w)	353	323	333	320	3.54	1.66	0.22	0.12	1.02	0.45	1.34	0.12	8.71	1.29	βb CCC(77)
	294(vw)	346	319	327	316	2.31	2.11	0.14	0.15	0.42	1.01	1.30	0.91	8.62	9.94	βb CCC(72)
	294(vw)	339	312	320	309	1.37	2.43	0.08	0.17	2.58	0.67	0.21	1.14	1.44	12.90	C-CH3 sci(47)
	294(vw)	310	283	293	281	1.11	1.13	0.05	0.06	26.46	0.22	0.40	0.01	3.19	0.13	twist NH2 (85)
	272(vw)	273	274	273	272	1.16	1.61	0.05	0.07	2.42	2.36	0.19	0.28	1.60	3.88	βb CCC(71)
		266	252	253	250	1.29	1.49	0.05	0.06	0.42	3.19	0.29	0.18	2.79	2.86	twist C-CH3 (81)
		264	243	251	241	1.34	1.28	0.05	0.05	0.24	1.92	0.31	0.06	3.17	1.01	twist C-CH3 (66)
		248	236	236	234	1.60	1.09	0.05	0.04	0.88	4.47	0.12	0.22	1.29	3.89	ν CC(55)
		212	199	211	197	1.14	3.16	0.03	0.08	2.19	0.41	0.11	0.28	1.57	6.59	twist C-CH3 (69)
	190(vw)	134	199	122	197	3.33	1.53	0.08	0.02	2.43	14.06	0.18	0.06	2.57	1.41	twist C-CH3 (78)
	136(vw)	128	130	128	129	2.55	1.91	0.03	0.02	0.57	8.16	0.15	0.05	4.46	2.45	C-CH3 rock(30)
		119	126	119	122	2.63	1.88	0.02	0.02	0.00	1.07	0.19	0.04	6.24	2.17	C-CH3 rock(45)

Intensities: w-weak, vw-very weak, s-strong, vs-very strong.

ν-stretching, ss-symmetric stretching, ass-asymmetric stretching, sd-in-plane bending, ad-out-of-plane bending, sciss.-scissoring, wag.-wagging, rock.-rocking, ipd-in-plane bending, opd-out-of-plane bending, ipr.-in-plane rocking, opr.-out-of-plane rocking, twist.-twisting, δ_{ring} - ring in-plane-bending, γ_{ring} - ring out-of-plane-bending
[a] Calculated by B3LYP/6-311+G**
[b] Calculated by HF/6-311++G**

Table 6: Natural bond orbital analysis of ATMP

Bomd (A-B)	ED/Energy a.u.	ED_A(%)	ED_B(%)	NBO	S(%)	P(%)
BD (N1-C2)	1.9769	60.27	39.73	0.7763 ($sp^{2.36}$) N+0.6303 ($sp^{3.67}$) C	29.75	21.39
BD (N1-C6)	1.9798	60.09	39.91	0.7752 ($sp^{2.28}$) N+0.6317 ($sp^{3.53}$) C	30.45	22.06
BD (N1-H7)	1.9796	67.61	32.39	0.8222 ($sp^{3.50}$) N+0.5691 ($sp^{0.00}$) H	22.21	99.94
BD (C2-C3)	1.9693	50.78	49.22	0.7126 ($sp^{2.66}$) C+0.7016 ($sp^{2.71}$) C	27.31	26.97
BD (C2-C8)	1.9760	51.41	48.59	0.7170 ($sp^{2.35}$) C+0.6971 ($sp^{2.41}$) C	25.95	29.33
BD (C2-C12)	1.9789	49.94	50.06	0.7067 ($sp^{2.69}$) C+0.7075 ($sp^{2.41}$) C	25.22	29.34
BD (C3-C4)	1.9618	48.77	51.23	0.6983 ($sp^{2.76}$) C+0.7158 ($sp^{4.63}$) C	26.60	17.75
BD (C4-C5)	1.9768	51.55	48.45	0.7180 ($sp^{1.77}$) C+0.6961 ($sp^{2.89}$) C	36.12	25.72
BD (C4-N19)	1.9872	40.62	59.38	0.6374 ($sp^{3.61}$) C+0.7706 ($sp^{1.73}$) N	21.67	36.66
BD (C5-C6)	1.9648	50.08	49.92	0.7076 ($sp^{2.74}$) C+0.7066 ($sp^{2.87}$) C	26.75	25.80
BD(C6-C24)	1.9795	50.34	49.66	0.7095 ($sp^{2.92}$) C+0.7047 ($sp^{2.42}$) C	25.49	29.20
BD (C2-C28)	1.9775	51.45	48.55	0.7173 ($sp^{2.77}$) C+0.6968 ($sp^{2.42}$) C	26.52	29.21
LP) (1) N1	1.9280			($sp^{4.71}$) N	17.51	
LP) (1) N19	1.9636			($sp^{36.17}$) N	2.690	
BD* (N1-C2)	0.0410	39.73	60.27	0.6303 ($sp^{2.36}$) N-0.7763 ($sp^{3.67}$) C	29.75	21.39
BD* (N1-C6)	0.0388	39.91	60.09	0.6317 ($sp^{2.28}$) N-0.7752 ($sp^{3.53}$) C	30.45	22.06
BD* (C2-C3)	0.0392	49.22	50.78	0.7016 ($sp^{2.66}$) C-0.7126 ($sp^{2.17}$) C	27.31	26.97
BD* (C2-C8)	0.0235	48.59	51.41	0.6971 ($sp^{2.85}$) C-0.7170 ($sp^{2.41}$) C	25.95	29.33
BD*(C2-12)	0.0397	50.06	49.94	0.7075 ($sp^{2.96}$) C-0.7067 ($sp^{2.41}$) C	25.22	29.34
BD* (C3-C4)	0.0303	51.23	48.77	0.7158 ($sp^{2.76}$) C-0.6983 ($sp^{4.63}$) C	26.6	17.75
BD* (C4-C5)	0.0194	48.45	51.55	0.6961 ($sp^{1.77}$) C-0.7180 ($sp^{2.89}$) C	36.12	25.72
BD*(C4-19)	0.0197	59.38	40.62	0.7706 ($sp^{3.16}$) C-0.6374 ($sp^{1.73}$) N	21.67	36.66
BD* (C5-C6)	0.0311	49.92	50.08	0.7066 ($sp^{2.74}$) C-0.7076 ($sp^{2.87}$) C	26.75	25.8
BD*(C6-C24)	0.0228	49.66	50.34	0.7047 ($sp^{2.92}$) C-0.7095 ($sp^{2.42}$) C	25.49	29.20
BD*(C6-C28)	0.0048	48.55	51.45	0.6968 ($sp^{2.77}$) C-0.7173 ($sp^{2.42}$) C	26.52	29.21

Perturbation theory analysis

Natural Bond Orbital (NBO) analysis provides an efficient method for studying intra-intermolecular bonding and charge transfer (or) conjugative interaction in molecular systems. Some electron donor, acceptor orbital's and stabilization energy resulted from the second-order micro-disturbance theory are reported [48]. The large $E^{(2)}$ value indicate the more intensive interaction between the electron-donors and electron-acceptors, i.e. the more donating tendency from electron donors to electron acceptors and greater the extent of conjugation of the whole system. The possible intensive interactions are given in Table 7 for ATMP. The second-order perturbation theory analysis of Fock matrix in NBO basis shows strong intramolecular hyperconjugative interactions of π electron. The LP-π conjugation between the N lone pair electrons and piperazine ring π system is strong in the ground state. The stabilization energy $E^{(2)}$ associated with hyperconjugative interactions C_{24}-H_{28} → C_{12}-H_{14} is seen to give a strong stabilization 58.69kJ/mol. This strong stabilization denotes the larger delocalization. The interesting interactions in ATMP compound are LP (N1)→ BD* (C_2 - C_{12}), LP (N_1)→ BD* (C_6–C_{24}), LP (N_{19})→ BD* (C_3–C_4), LP(N_{19})→ BD* (C_2–C_3),LP(N_{19})→ BD* (C_4–H_{18})are obtained as 7.17, 6.84, 2.94, 3.4, and 1.57(kJ/mol), respectively. This highest interaction around the ring can induce the large bioactivity in the compound. The p-character of nitrogen lone pair orbital LP(N1) and LP(N19) are 82.44% and 97.30% respectively. This shows that the lone pair orbital participates in electron donation in the compound.

Mulliken charge analysis

The charge distribution on molecule has significant influence in vibrational spectra. Mulliken net charges calculated at the B3LYP level with the 6-311+G(d,p) atomic basis set using Gaussian 09 are shown in Fig. 5. The charge distribution of ATMP was calculated from the atomic charges by NLO and NBO analysis (Fig. 5). These two methods predict the same trend i.e., among the nitrogen atoms N1 and N19 is considered as more basic site [49]. The charge distribution shows that the more negative charge is concentrated on N19 atom whereas the partial positive charge resides at hydrogens. When compared to nitrogen and carbon atoms (N1, N19, C3, C5, C8 and C24), hydrogen atoms (H30 and H31) are less electronegative and it can be seen from the bar diagram [50].

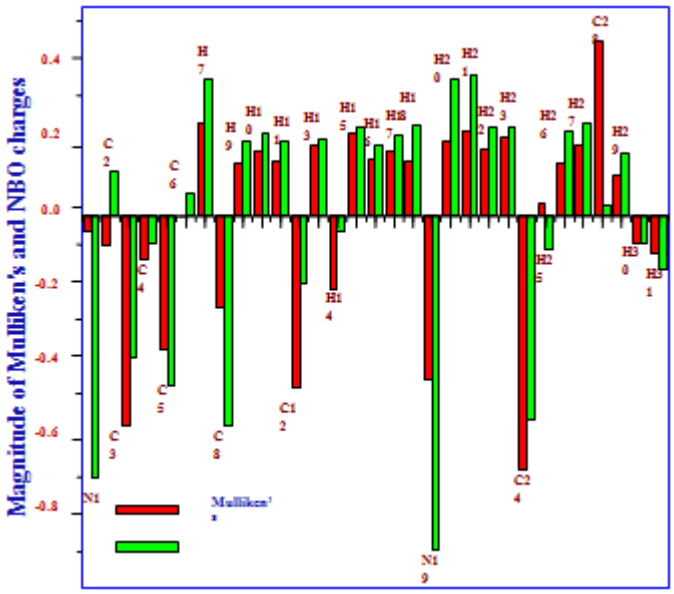

Figure 5: Comparative graph of Mulliken's vs. natural atomic charges

Fukui function

The condensed Fukui functions (f_k) were calculated using the simple procedure (based on Mulliken population analysis) given by Yang and Mortier [51]. For a system of N electrons, independent calculations are to be made for corresponding N+1, N-1 and N are total electrons present in anion, cation and neutral state of molecules respectively. Mulliken population analysis yields gross charges $q_k(N+1)$, $q_k(N-1)$, $q_k(N)$ and for all atoms k. In a finite-difference approximation, the condensed Fukui functions $f_k^+ = q_k(N+1) - q_k(N)$ for nucleophilic attack, $f_k^- = q_k(N) - q_k(N-1)$ for electrophilic attack and $f_k^0 = ½[q_k(N+1) - q_k(N-1)]$ for free radical attack, where $q_k$is the electronic population of atom k in the molecule, N the number of electrons, were calculated. Morell et al. [52] have recently proposed a dual descriptor ($\Delta f(r)$), which is defined is defined as the difference between the nucleophilic and electrophilic Fukui function and is given by the equation,

$$\Delta f(r) = [f^+(r) - f^-(r)]$$

$\Delta f(r) > 0$,

then the site is favored for a nucleophilic attack, whereas if $\Delta f(r) < 0$, then the site may be favored for an electrophilic attack. According to dual descriptor $\Delta f(r)$ provide a clear difference

Table 8: Local reactivity descriptors (au) of ATMP

Atom	*Electronic population* $q_k(N-1)$	q_k *(N)*	q_k *(N+1)*
N1	1.179	-0.535	0.812
C2	-0.079	-1.261	0.812
C3	-0.809	-1.015	-0.502
C4	-1.098	0.473	-0.651
C5	0.195	1.258	-0.502
C6	0.869	0.885	0.812
H7	1.706	-0.768	-0.029
C8	-0.596	-2.144	1.963
H9	0.108	-2.127	2.769
H10	-1.539	-1.770	2.304
H11	-0.715	-3.149	1.616
C12	0.609	-2.509	0.229
H13	1.550	-2.658	0.716
H14	-0.013	-3.365	0.385
H15	0.768	-2.371	-0.820
H16	-0.197	-1.342	-1.316
H17	-1.730	-1.559	-0.506
H18	-1.676	0.729	-1.978
N19	-1.077	0.881	-2.764
H20	-2.669	0.752	-2.095
H21	-1.791	0.779	0.105
H22	0.849	1.026	-1.316
H23	-0.021	2.306	-0.506
C24	1.176	1.862	1.963
H25	2.103	2.360	1.771
H26	0.390	2.585	2.036
H27	1.247	1.318	2.882
C28	2.255	1.216	0.228
H29	2.957	0.466	0.528
H30	2.195	1.240	-0.840
H31	1.179	-0.535	0.812
Fukui function		Local softness	
f_k^-	f_k^+	s_k^-	$s_k^{\mp}$
-1.182	1.347	-11.441	13.039
-0.206	2.073	-1.993	20.072
1.572	0.513	15.215	4.964
1.063	-1.124	10.291	-10.885
0.016	-1.760	0.151	-17.039
-2.474	-0.073	-23.949	-0.705
-1.548	0.738	-14.989	7.147
-2.234	4.107	-21.631	39.766
-0.231	4.896	-2.241	47.402
-2.434	4.074	-23.560	39.447
-3.118	4.765	-30.185	46.132
-4.208	2.737	-40.738	26.502
-3.352	3.374	-32.453	32.662
-3.139	3.750	-30.388	36.307
-1.145	1.550	-11.089	15.007
0.170	0.026	1.647	0.251
2.405	1.053	23.289	10.197
1.957	-2.707	18.950	-26.212
3.421	-3.645	33.120	-35.287
2.570	-2.847	24.886	-27.565
0.177	-0.675	1.715	-6.532
2.327	-2.343	22.533	-22.679
0.686	-2.812	6.640	-27.224
0.257	0.102	2.489	0.983
2.194	-0.589	21.244	-5.704
0.072	-0.549	0.696	-5.315
-1.039	1.564	-10.064	15.140
-2.491	-0.988	-24.116	-9.567
-0.955	0.062	-9.243	0.599
-0.406	-2.081	-3.928	-20.146
-1.182	1.347	-11.441	13.039

That is they provide positive value for sited prone for nucleophilic attack and a negative value prone for electrophilic attack. From the values reported in Table 8, according to the condition for dual descriptor, nucleophilic site for in our title molecule is N1, C2, C6, H7, C8, H9, H10, H11, C12, H13,H14, H15, H27, C28, H29 and H31 (Positive value i.e. $\Delta f(r) > 0$). Similarly the electrophilic site is C3, C5, H16, H17, H18, N19, H20, H21, H22, H23, H24, H25, H26, H27, C28 and H30 (Negative value i.e. $\Delta f(r) < 0$). The behavior of molecule as electrophilic and nucleophilic attack during reaction depends on the local behavior of molecule.

Solvent effect on the UV/vis spectrum

The calculations of electronic structures of the title compound were carried out using TD-DFT calculations with the B3LYP/6-311+G (d, p) method. Before the electronic calculations, the molecule was optimized in ground state using the DFT method with B3LYP functional. It is obvious that the use of TD-DFT calculations for prediction of the electronic absorption spectra is a reasonable method. The calculated results involving the vertical excitation energies, oscillator strength (f), wavelength (λ) and life span (τ) for gas phase and various solvents are illustrated in Table 9.

Table 9: Maximum absorption wavelength (nm), excitation energies E (eV), oscillator strength (f) of ATMP and life span time (ls) of its first and second excited state derived from calculation in different media using DFT/B3LYP/6-311++G(d,p) method

Solvents	λ (nm)	Energy (eV)	Osc. Strength (*f*)	Micro-transition (contribution in %)	Life-span ×10−7s
Gas	261	4.215	0.0272	HOMO→LUMO(86%)	
				HOMO→L+1(2%)	0.37
				HOMO→L+2(6%)	
				HOMO→L+3(5%)	
	237	4.727	0.005	HOMO→L+1(91%)	
				HOMO→LUMO(3%)	
	231	4.812	0.0037	HOMO→LUMO(10%)	
				HOMO→L+2(54%)	
				HOMO→L+3(24%)	
				HOMO→L+4(7%)	
Choloro-form	327	3.786	0.0103	HOMO→LUMO(95%)	1.68
				HOMO→L+1(4%)	
	261	4.751	0.0198	HOMO→L+1(63%)	
				HOMO→L+3(12%)	
				HOMO→L+4(14%)	
				HOMO→LUMO(2%)	
				HOMO→L+2(4%)	
	257	4.829	0.0114	HOMO→L+1(16%)	
				HOMO→L+2(51%)	
				HOMO→L+3(25%)	
DMSO	325	3.814	0.0112	HOMO→LUMO (95%)	2.17
				HOMO→L+1(4%)	
	259	4.787	0.019	HOMO→L+1(73%)	
				HOMO→L+4(13%)	
				HOMO→LUMO(3%)	
				HOMO→L+3(5%)	
	255	4.854	0.0155	HOMO→L+2(33%)	
				HOMO→L+3(49%)	
				HOMO→L+1(9%)	
				HOMO→L+4(3%)	
				HOMO→L+8(2%)	

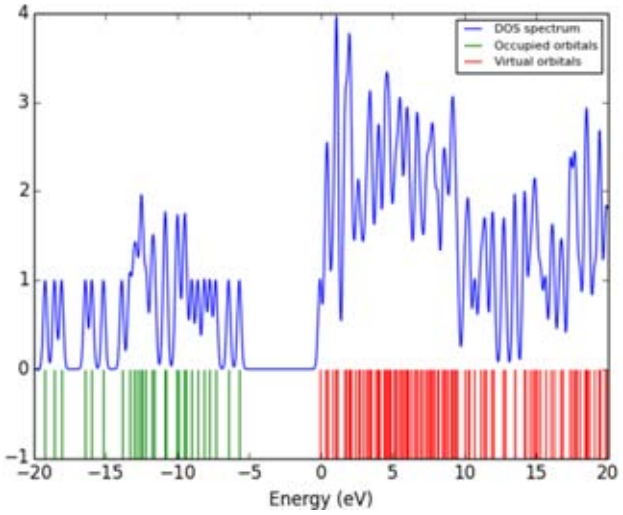

Figure 6: Density of states (DOS) diagram of ATMP

Calculated λ_{max} values obtained with B3LYP/6-311+G (d, p) are 261, 237 and 231 nm in gas which are HOMO →LUMO, HOMO→ LUMO+1, HOMO→ LUMO+2, HOMO→ LUMO+3 and HOMO→ LUMO+4 transitions, respectively. In chloroform and DMSO, these values are calculated at 327, 261, 257 and 325, 259, 255 nm which are the same transition in, chloroform and DMSO, respectively is shown in Table 9.

Gauss-Sum 2.2 program [53] was used to calculate group contributions to the molecular orbitals (HOMO and LUMO) and prepare the density of states (DOS) spectrum in Fig.6. The DOS spectra were created by convoluting the molecular orbital information with GAUSSIAN curves of unit height. The green and blue lines in the DOS spectrum indicate the HOMO and LUMO levels. Fig 6, illustrates molecular orbitals involved in the different transitions leading to observed peaks in ATMP.

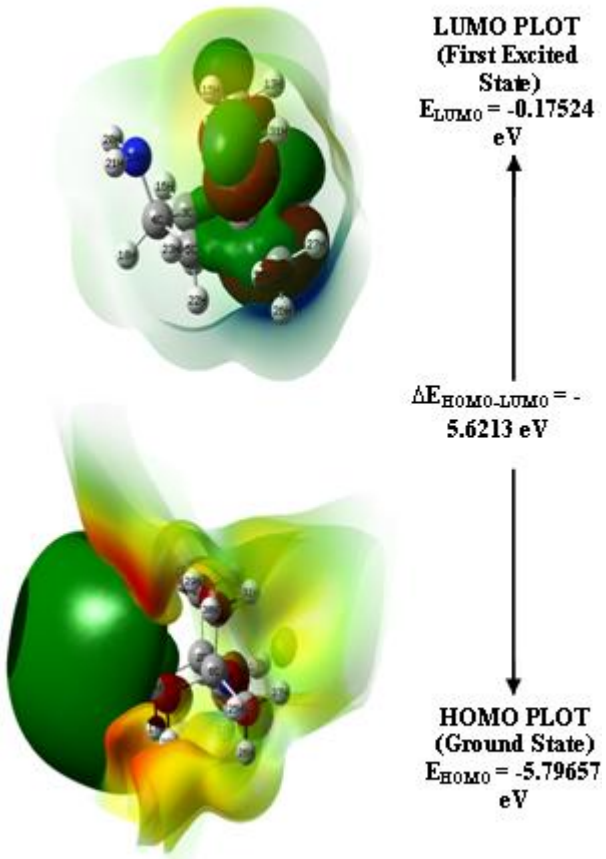

Fig. 7 The frontier molecular orbitals

Frontier molecular orbital

The most important frontier molecular orbital (FMO) such as higher occupied molecular orbital (HOMO) and lowest unoccupied molecular orbital (LUMO) plays a crucial part in the chemical stability of the molecule [54]. The HOMO represents the ability to donate an electron and LUMO as an electron acceptor represents the ability of accept an electron [55]. The energy gap between HOMO and LUMO also determines the chemical reactivity, optical polarizability and chemical hardness–softness of a molecule [55].

In the present study, the HOMO and LUMO energies are predicted at B3LYP level with the 6-311+G(d,p) basis set. Our calculation predicts that there are 362 molecular orbits present in title molecules with energy ranges -388.94 eV to 970.17eV among them 44 orbits are occupied and rest are unoccupied. The highest occupied molecular orbital (HOMO) and the lowest unoccupied molecular orbital (LUMO) have energies -5.79657 eV and -0.17524 eV for ATMP. The difference between HOMO and LUMO is 5.6213 eV. An electron makes transition from LUMO to HOMO resulting FT-Raman spectra of wavenumber 1584 cm^{-1}. However, the energy difference between LUMO and ground state is -388.94 eV, i.e., transition between LUMO and ground state of ATMP emits FT-Raman spectra of wavenumbers 136 cm^{-1}.

Global reactivity descriptors

The molecular quantities such as ionization potential(I), electron affinity (A), chemical potential (μ), electronegativity (χ), absolute hardness (η), global softness (σ) and global electrophilicity (ω). The chemical potential (μ) of the electrons (the negative of the electronegativity χ) is given by

Table 10: Quantum chemical parameter of ATMP

Chemical parameter	*Monomer*
Ionization potential(I) (eV)	5.79657
Electron affinity(A) (eV)	0.17524
Global hardness(η) (eV)	5.62133
Global softness (S) (eV)	0.17789
Chemical potential(μ) (eV)	−2.98595
Electrophilicity (ω) (eV)	0.79304
Electro negativity(χ) (eV)	2.98595

$$M = \left(\frac{\partial E}{\partial N}\right)_{v(r)}$$

$$\mu = -\frac{1}{2}(I + A)$$

and it has the same value everywhere [56]. In a finite-difference approximation:

$$\chi = -\mu = \frac{1}{2}(I + A)$$

were I and A are the ionization potential and electron affinity. The change of μ with the number of electrons was defined by Parr and Pearson as a measure for the "absolute hardness" as

$$\eta = \left(\frac{\partial \mu}{\partial N}\right)_{v(r)} = \left(\frac{\partial^2 E}{\partial N^2}\right)_{v(r)}$$

[57] The corresponding finite-difference formula is

$$\eta = \frac{1}{2}(I + A)$$

The softness (σ) is reciprocal of the hardness (η)

The electrophilicity index can be estimated by the equation [58]:

$$\omega = \frac{\mu^2}{2\eta}$$

Thus the frontier molecular orbital analysis and global reactivity parameters of the molecule in B3LYP and LSDA methods with 6-311+G(d,p) basis set are presented in Table 10, respectively.

Molecular electrostatic potential

In the present study, 3D plots of molecular electrostatic potential (MEP) of ATMP is illustrated in Fig 8. The MEP which is a plot of electrostatic potential mapped onto the constant electron density surface with together HOMO and LUMO (Fig.7). The MEP is a useful property to study reactivity given that an approaching electrophile will be attracted to negative regions (where the electron distribution effect is dominant). The importance of MEP lies in the fact that it simultaneously displays molecular size, shape as well as positive, negative and neutral electrostatic potential regions in terms of color grading (Fig 8) and is very useful in research of molecular structure with its physiochemical property relationship [59,60]. The different values of the electrostatic potential at the surface are represented by different colors. Potential increases in the order red < orange < yellow < green < blue. The color code of these maps is in the range between –1.2908a.u. (deepest red) to 0.1498a.u. (deepest blue) in compound, where blue indicates the strongest attraction and red indicates the strongest repulsion. MEPs color scale is such $\delta^+ \rightarrow \delta^-$ in the direction red → blue. As can be seen from the MEP map of the title molecule, while regions having the negative potential are over the electronegative atoms (Nitrogen atom), the regions having

the positive potential are over the carbon and hydrogen atoms. The negative potential value is -18.4292 and -18.4208a.u. for nitrogen atoms (N1 and N19). A maximum less negative region localized on

	V(r)	Point Charges (e)
N19	-18.4292	-1.2908
N1	-18.4208	-0.9632
C24	-14.8190	-0.3655
C12	-14.8183	-0.3461
C3	-14.8001	-0.3932
C8	-14.7997	-0.5295
C28	-14.7955	-0.5528
C5	-14.7709	-0.3079
C4	-14.7524	0.3471
C2	-14.7450	0.7340
C6	-14.7312	0.5504
H17	-1.1473	0.0950
H27	-1.1381	0.0419
H10	-1.1349	0.1307
H15	-1.1338	0.0232
H11	-1.1309	0.1138
H29	-1.1304	0.1440
H9	-1.1285	0.1059
H31	-1.1269	0.1433
H30	-1.1253	0.1306
H26	-1.1252	0.1015
H13	-1.1244	0.0660
H16	-1.1230	0.1422
H23	-1.1210	0.1191
H22	-1.1165	0.1626
H18	-1.0882	0.0902
H7	-1.0704	0.3858
H21	-1.0638	0.4452
H20	-1.0619	0.4706
H25	-1.0473	0.0560
H14	-1.0458	0.1498

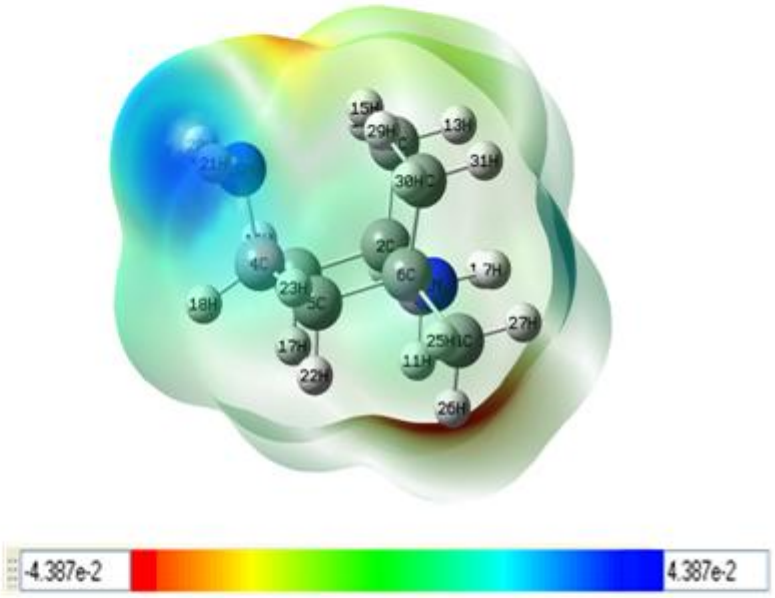

Fig. 8 Molecular electrostatic potential (MEP) surface map for ATMP

the hydrogen atom bond has value of -1.0458a.u. From these results, we can say that the carbon (H_{14}) atom indicates the strongest attraction and nitrogen atom indicates the strongest repulsion.

Thermodynamic analysis

In consideration of the dependence of association constant (K_a) on temperature, a thermodynamic process was considered to be responsible for the intermolecular interactions. The molecular forces contributing to biomolecules interaction with small molecules substrates may involve hydrogen bond, van der Waals force, hydrophobic interaction force, and electrostatic force [61]. The thermodynamic parameters, enthalpy change (ΔH) and entropy change (ΔS)of reaction are main evidence for characterizing the acting force. If there is no significant change in temperature, ΔH and ΔS can be estimated from the van't Hoff equation as follows:

$$\log K_a = \frac{\Delta H}{2.303RT} + \frac{\Delta S}{2.303RT}$$

were *R* is the gas constant, and the temperatures used were 100, 200, 298.15, 300, 400, 500 K. The values of ΔH and ΔS were obtained from spectroscopic data by statistical methods. The value of free energy change (ΔG) can be calculated from the following equation:

$$\Delta G=\Delta H-T\Delta S$$

Table 11 lists the thermodynamic parameters for the interaction of ATMP. The negative values of ΔG revealed that the binding process was spontaneous.

Table 11: Thermodynamic parameters of ATMP at different temperatures by B3LYP/6-311++G(d,p) method.

Temp (K)	Cp (kcal/mol)	ΔH (kcal/mol)	ΔS (kcal/mol)	ΔG (kcal/mol)
100	19.4629	8.3020	67.8802	-6779.7153
200	37.3134	11.1841	81.3773	-16264.267
298.15	53.8955	16.5286	81.3773	-24246.100
300	54.2133	16.6478	96.6168	-28968.385
400	70.9578	23.8925	113.2716	-45284.746

5. Conclusion

HF and B3LYP level with the 6-311+G(d,p) basis sets are utilized to conduct a detailed study of the structures, geometrical parameters, molecular electrostatic potential map and thermodynamic parameters of ATMP. Comparison between the calculated and experimental structural parameters indicates that B3LYP/6-311+G(d,p) results are in good agreement with experimental values. The vibrational spectra of ATMP were found to be in good agreement with calculated values. It is seen from the theoretical results, there is no remarkable difference between the results of the DFT level used in evaluating geometrical parameters and vibrational frequencies. The significant changes in bond lengths of the ATMP have been explained with the help of NBO analysis. The delocalized of ED from Lewis to non-Lewis sites are discussed with their stabilization energies. The lowering of the HOMO–LUMO energy gap value has substantial influence on the intra molecular charge transfer and bioactivity of the molecules. The MEP map is agrees well with the ground state interaction. The electro negativity, hardness and electrophilicity were found. The Fukui functions showed that the ring and substitution atoms are the most probable sites for electrophilic and free radical attacks. The correlations between the statistical thermodynamics properties are also obtained.

6. Acknowledgement

This work was supported by the University Grants Commissions fund through research Grant no.: MRP-5124/14 (SERO/UGC).

References

[1] V. Vinayak, Kane and Maitland Jones Jr (1990). "Spiro[5.7]trideca-1,4-dien-3-one". Org. Synth.; Coll. Vol. **7**, p. 473
[2] B. Michael, Smith, Jerry March (2001).March's Advanced Organic Chemistry: Reactions, Mechanisms, and Structure (5th *ed.*). Wiley-Interscience. ISBN 0-471-58589-0.
[3] P. George. Claxton, Lloyd Allen, and J. Martin Grisar (1988). "2,3,4,5-Tetrahydropyridine trimer". Org. Synth.; Coll. Vol. **6**, p. 968
[4] C. S. Marvel and W. A. Lazier (1941). "Benzoyl Piperidine". Org. Synth.; Coll. Vol. **1**, p. 99
[5] Spaeth and Englaender, Ber.1935,68, 2218; cf. Pictet; Pictet (1927). Helv. Chim. Acta**10**: 593.
[6] Rimington (1934). S. Afr. J. Sci**31**: 184.
[7] Juraschewski; Stepanov (1939). J. Gen. Chem., U.R.S.S. **9**: 1687.
[8] J.L. Arbiser, T. Kau, M. Konar, et al. (2007). "Solenopsin, the alkaloidal component of the fire ant (Solenopsisinvicta), is a naturally occurring inhibitor of phosphatidylinositol-3-kinase signaling and angiogenesis". Blood **109** (2): 560–5. doi:10.1182/blood-2006-06-029934. PMC 1785094. PMID 16990598.
[9] Thomas Anderson Henry (1949). The Plant Alkaloids (4th ed.). The Blakiston Company
[10] Karsten Eller, Erhard Henkes, Roland Rossbacher, HartmutHöke "Amines, Aliphatic" Ullmann's Encyclopedia of Industrial Chemistry 2002 Wiley-VCH. doi:10.1002/14356007.a02_001
[11] M. J. Frisch, ed al., Gaussian, Inc., Wallingford CT, 2009
[12] A.D. Becke, Phys. Rev. A 39 (1988) 3098−3100.
[13] C. Lee, W. Yang, G.R. Parr, Phys. Rev. B 37 (1998) 785−789.
[14] A. Frich, A.B. Nielsen, A.J. Holder, Gaussview Users Manual, Gaussian Inc., Pittsburgh, 2007.
[15] G. Fogarasi, P. Pulay, in: J.R. Durig(Ed.), Vibrational Spectra and Structure, vol.14, Elsevier, Amsterdam, 1985, p. 125.
[16] P. Pulay, G. Fogarasi, F. Pongor, J.E. Boggs, A. Vargha, J. Am. Chem. Soc. 105 (1983) 7037.
[17] T. Sundius, J. Mol. Struct. 218 (1990) 321−326.
[18] T. Sundius, Vib. Spectrosc.29 (2002) 89−95.
[19] E.D.Glendering, A.E. Reed, J.E. Carpenter, F. Weinhold, NBO Version 3.1, TCI, University of Wisconsin, Madison, 1998.
[20] A.E. Reed, L.A. Curtiss, F. Weinhold, Chem. Rev. 88 (1988) 899–926.
[21] F. Weinhold, J.E. Carpenter, The Structure of Small Molecules and Ions, Plenum, New York, 1988.
[22] C. Muñoz-Caro, A. Niño, M.L. Senent, J.M. Leal, S. Ibeas, J. Org. Chem. 65 (2000) 405–410.
[23] S. Miertus, E. Scrocco, J. Tomasi, Theor. Chem. Acc. 103 (2000) 343–345
[24] P. Politzer, J. Murray, Theor. Chem. Acc. 108 (2002) 134–142
[25] P.L. Polavarapu, J. Phys. Chem. 94 (1990) 8106−8112.
[26] G. Keresztury, S. Holly, J. Varga, G. Besenyei, A.Y. Wang, J.R. Durig, Spectrochim, Acta A 49(1993) 2007−2026.
[27] D.A. Kleinman, Phy. Rev. 126 (1962) 1977.
[28] S. K. Goswami, L. R. Hanton, C. J. McAdam, S. C. Moratti and J. Simpson, *Acta Cryst.* (2011). E67, o3024-o3025
[29] Yu.A. Pentin, O.S. Anisimova, *Opt. Spectrosc.* **26**, 1968, *35*.

[30] T. Hirakowa, T. Kimura, K. Ohno, H. Murata, *Spectrochim. Acta A* **36**, 1980, 329–332.
[31] G. Gundersen, D.W. Rankin, *Acta Chem. Scand. A* **37**, 1983, 865–874.
[32] MOLVIB: A Program for Harmonic Force Field Calculations, QCPE Program No. 807, 2002.
[33] N. B. Colthup, L.H. Daly, S.E. Wiberley, Introduction to Infrared and Raman Spectroscopy, Academic Press, New York, 1990.
[34] G. Socrates, Infrared, Raman Characteristic Group Frequencies, Tables and Charts, Third ed., Wiley, Chichester, 2001.
[35] D. Lin-Vein, N.B. Colthup, W.G. Fately, J.G. Grasselli, The Handbook of Infrared and Raman Characteristic Frequencies of Organic Molecules, Academic Press, New York, 1991
[36] M. Gussoni, C. Castiglioni, J. Mol. Struct. 521 (2000) 1-18.
[37] N.B. Colthup, L.H. Daly, S.E. Wiberley, Introduction to Infrared and Raman Spectroscopy, Academic Press, New York, 1990.
[38] B.C. Simith, Infrared Spectral Interpretation, CRC Press, Boca Raton, FL, 1996.
[39] L.J. Bellamy, The Infrared Spectra of Compound Molecules, Chapman and Hall, London, 1975.
[40] D. Sajan, J. Binoy, B. Pradeep, K. Venkatakrishnan, V. Kartha, I. Joe, V. Jayakumar, 2004. Spectrochim.ActaA 60: 173-180.
[41] Fundamentals of Molecular Spectroscopy, Colin N. Banwell and Elaine M. McCash, Tata McGraw-Hill reprint 1995.
[42] G. Socrates, Infrared Characteristics Group Frequencies, John Wiley, GB, 1980.
[43] S. Ahmad, P.K. Verma, Ind. J. Phys. B 64 (1990) 50–55
[44] D.N. Sathyanarayana, Vibrational Spectroscopy Theory and Applications(New Age, International, New Delhi) 1996
[45] M. Snehalatha, C. Ravikumar, I. Hubert Joe, V.S. Jayakumar, J. Raman Spectrosc.40 (2009) 1121–1126.
[46] A.E. Ledesma, J. Zinczuk, A. Ben Altabef, J.J. Lopez Gonzalez, S.A. Brandhan, J.Raman Spectrosc. 40 (2009) 1004–1010.
[47] J. Chocholoušová, V. Vladimír Špirko, P. Hobza, Phys. Chem. Chem. Phys. 6 (2004) 37–41.
[48] J.N. Liu, Z.R. Chen, S.F. Yuan, J. Zhejiang Univ, Science B 6 (2005) 584–589.
[49] P. Wang, P. Zhu, W. Wu, H. Kang, C. Ye, Phys. Chem. Chem. Phys. 1 (1999) 3519.
[50] G. Wang, F. Lian, Z. Xie, G. Su, L. Wang, X. Jing, F. Wang, Synth. Met. 131 (2002)1.
[51] W. Yang, W.J. Mortier, J. Am. Chem. Soc. 108 (1986) 5708–5711.
[52] C. Morell, A. Grand, A. Toro-Labbe, J. Phys. Chem. A 109 (2005) 205–212.
[53] N.M. O'Boyle, A.L. Tenderholt, K.M. Langer, J. Comput. Chem. 29 (2008) 839–845.
[54] B. Kosar, C. Albayrak, Spectrochim. Acta 78A (2011) 160–167.
[55] P. Senthil kumar, K. Vasudevan, A. Prakasam, M. Geetha, P.M. Anbarasan, Spectrochim. Acta 77A (2010) 45–50.
[56] (a) R.G. Parr, W. Yang, J. Am. Chem. Soc. 106 (1984) 4049–4050;
a. (b) W. Yang, R.G. Parr, R. Pucci, J. Chem. Phys. 81 (1984) 2862–2863.
[57] R.G. Parr, R.A. Donnelly, M. Levy, W.E. Palke, J. Chem. Phys. 68 (1978) 3801–3807.
[58] R.G. Parr, R.G. Pearson, J. Am. Chem. Soc. 105 (1983) 7512–7516.
[59] J.S. Murray, K. Sen, Molecular Electrostatic Potentials, Concepts and 399 Applications, Elsevier, Amsterdam, 1996.
[60] E. Scrocco, J. Tomasi, in: P. Lowdin (Ed.), Advances in Quantum Chemistry, Aademic Press, New York, 1978.
[61] N. Akbay, Z. Seferoglu. E. Gok, J. Fluoresc. 19(2009) 1045-1051.